SANDIA REPORT

SAND2014-17174
Unlimited Release
Printed September 2014

Hydrogen Isotope Exchange in a Metal Hydride Tube

David B. Robinson

Prepared by
Sandia National Laboratories
Albuquerque, New Mexico 87185 and Livermore, California 94550

Sandia National Laboratories is a multi-program laboratory managed and operated by Sandia Corporation, a wholly owned subsidiary of Lockheed Martin Corporation, for the U.S. Department of Energy's National Nuclear Security Administration under contract DE-AC04-94AL85000.

Issued by Sandia National Laboratories, operated for the United States Department of Energy by Sandia Corporation.

Available to DOE and DOE contractors from
U.S. Department of Energy
Office of Scientific and Technical Information
P.O. Box 62
Oak Ridge, TN 37831

Telephone: (865) 576-8401
Facsimile: (865) 576-5728
E-Mail: reports@adonis.osti.gov
Online ordering: http://www.osti.gov/bridge

Available to the public from
U.S. Department of Commerce
National Technical Information Service
5285 Port Royal Rd.
Springfield, VA 22161

Telephone: (800) 553-6847
Facsimile: (703) 605-6900
E-Mail: orders@ntis.fedworld.gov
Online order: http://www.ntis.gov/help/ordermethods.asp?loc=7-4-0#online

SAND2014-17174
Unlimited Release
Printed September 2014

Hydrogen Isotope Exchange in a Metal Hydride Tube

David B. Robinson
Energy Nanomaterials Department
Sandia National Laboratories
P.O. Box 969
Livermore, California 94551-MS9291

Abstract

This report describes a model of the displacement of one hydrogen isotope within a metal hydride tube by a different isotope in the gas phase that is blown through the tube. The model incorporates only the most basic parameters to make a clear connection to the theory of open-tube gas chromatography, and to provide a simple description of how the behavior of the system scales with controllable parameters such as gas velocity and tube radius. A single tube can be seen as a building block for more complex architectures that provide higher molar flow rates or other advanced design goals.

ACKNOWLEDGMENTS

The author thanks Maher Salloum for his generous assistance with the COMSOL software, and Steve Rice, who helped identify important references. Stewart Griffiths provided early guidance on this topic. Work with Andrew Shugard on Ref. 9 provided insights beneficial to this work. Shugard and Weifang Luo provided helpful technical reviews of this document.

CONTENTS

FIGURES

TABLES

NOMENCLATURE

Acronyms

GC	Gas chromatography
DOE	Department of Energy
PLOT	Porous-layer open tube

Roman Symbols

A_c	Packed column cross-sectional area [cm^2]
A_g	Gas phase cross-sectional area within tube [cm^2]
A_g^*	Gas phase cross-sectional area within pore [cm^2]
A_s	Solid phase cross-sectional area within tube [cm^2]
A_g^*	Solid phase cross-sectional area within pore [cm^2]
B	Effective permeability of a porous medium [cm^2]
C_g	Gas phase molar concentration [mol/cm^3]
C_s	Solid phase molar concentration [mol/cm^3]
D	Gas-phase atomic concentration of eluent [mol/cm^3]
D_s	Solid-phase atomic concentration of eluent [mol/cm^3]
D	Gas-phase binary diffusion coefficient [cm^2/s]
D_s	Solid-phase binary diffusion coefficient [cm^2/s]
d_p	Diameter of solid-phase particle [cm]
E_a	Activation energy [J/mol]
$[H_2]$	Diatomic eluent concentration [mol/cm^3]
[HD]	Diatomic mixed-isotope concentration [mol/cm^3]
$[D_2]$	Diatomic eluate concentration [mol/cm^3]
H	Gas-phase atomic eluent concentration [mol/cm^3]
H_s	Solid-phase eluent concentration [mol/cm^3]
$\overline{H}_s$	Average solid-phase eluent concentration [mol/cm^3]
ID	Inner diameter of tube [cm]
K	First-order equilibrium constant
K_{HD}	Equilibrium constant for formation of HD
k	Reaction rate constant [mol/cm^2 s]
k'	Ratio of solid-phase to gas-phase capacity
L	Axial length of the compact [cm]
M	Gas molecular mass [g/mol]
n	Molar eluent capacity of tube [mol]
$\dot{n}$	Molar flow rate through tube [mol/s]
N	Number of theoretical plates
N_{opt}	Number of theoretical plates under optimal conditions
OD	Outer diameter of tube [cm]
P	total gas pressure [kPa]
ΔP	pressure loss across the tube [kPa]
q	tortuosity factor [dimensionless]
R	Reaction rate [mol/cm^2 s]
R_g	Universal gas constant [8.314 J/mol K]
r	Radial coordinate [cm]

r_0	Inner radius of tube [cm]
r_p	Radius of pore in stationary phase
S	Phase boundary surface area per unit length of tube [cm^2/cm]
S^*	Phase boundary surface area per unit length of pore [cm^2/cm]
T	Temperature [K]
t	Time [s]
t_{el}	Time to elute hydrogen from column [s]
v_0	Average gas velocity [cm/s]
v_k	Reaction rate parameter [cm/s]
v_m	Mean speed of gas molecules [cm/s]
v_{opt}	Optimal gas velocity [vm/s]
z	Axial coordinate [cm]

Greek Symbols

α	Isotope separation factor (second-order equilibrium constant)
δ	Solid-phase surface layer thickness [cm]
μ	Gas viscosity [Pa s]
ξ	Ratio of outside to inside tube diameter
ρ	Packed column density [g/cm^3]
ρ_{bulk}	Density of nonporous solid hydride [g/cm^3]
σ	Front width parameter [cm]
σ_{HD}	HD peak width [cm]
ϕ	Stationary phase void fraction (porosity)
ϕ_c	Packed column void fraction (porosity)

Some symbols appear that are intermediate mathematical parameters that do not have much physical significance. These include j_1, j_2, u_1, u_2, and u_3. Some variations of units are used (such as cm vs. m).

1. INTRODUCTION

In the 1950s, many advancements were made to the theory of chromatography. Among the significant milestones, Marcel Golay provided a description of gas chromatography in a tube coated on the inside with a sorbent material.[1] In gas chromatography (GC), a sample is introduced as a narrow plug at one end of the tube, and blown through with an inert carrier gas. One or more sample components bind reversibly to the sorbent material, moving through the tube at a reduced speed that is specific to each component. Several mechanisms cause broadening of the sample plug, including axial diffusion (when that process is fast), and radial diffusion and absorption/desorption (when those processes are slow). These lead to an optimal value for the flow rate of the carrier gas for a given tube geometry. A GC system of this geometry that operates under conditions that minimize broadening can separate sample components with greater speed, shorter columns, and lower pressures than columns made of packed-powder sorbent materials. For scientific studies of the sorption reactions, a well defined geometry can lead to more clearly defined measurements of reaction rates, because measured values are averaged over a narrower range of conditions. Open-tube gas chromatography is now a mature, commercialized chemical separation method that is well established in industry and research, with a market in the billion-dollar range.

Isotopic displacement has been studied in packed-powder columns by various authors. Palladium,[2,3,4,5] palladium alloy,[6,7] lanthanum-nickel alloy,[8] and uranium[9] hydrides are among the studied materials. The process is similar to GC, except that instead of pushing a plug of sample through the column, a boundary between the two isotopes is pushed through the column. A carrier gas is often not used. The displacement reaction is a bimolecular (second-order) chemical reaction, meaning that the rate of the reaction is proportional to the concentrations of two different species. GC is treated as first-order by Golay, where the rate of binding is proportional to the concentration of only the gas-phase species (though many nonlinear elaborations have been described[10,11]).

In packed-powder columns, gas flows through a distribution of channel widths, around a distribution of solid-phase depths, at a distribution of pressures; some of which may be far from the conditions that minimize broadening. It may be possible to construct a column with higher performance by fabricating flow channels with more well defined geometry, given a clearer understanding of what the optimal conditions are. To obtain this, it is necessary to understand how an analysis like Golay's can be extended to the case of a second-order reaction.

This report attempts to chart a rapid path to this, seeking the simplest set of assumptions that captures the dependence on designable parameters like channel geometry and flow rate, drawing heavily from the work of Vermeulen and others who studied second-order reactions in the context of packed-powder columns for ion-exchange chromatography. It first describes the physical situation and parameterization of the problem for both first-order and second-order reactions, and then examines the first-order case leading to Golay's results, and the optimal conditions that it predicts. Then the case of the second-order reaction is considered, along with the difference between the two.

In these treatments, the effect of slow mass transport in the solid phase is unrealistically ignored. That effect is considered in Chapter 5, where a remedy is proposed in which two types of tube are hierarchically arranged. Further elaborations are briefly discussed in Chapter 6, along with a comparison to the case of a packed-powder column.

2. DEFINITION OF MODEL SYSTEM

The scenario considered here is a tube with an open channel through the middle, an impenetrable outer wall, and a layer of metal hydride on the inside of the tube wall. A pure gas-phase hydrogen isotope differing from that in the metal hydride enters the left end of the tube with a defined velocity distribution. As gas flows down the tube, a chemical reaction occurs between the gas and the metal hydride, in which the initial isotope is displaced by the isotope that is flowing in. The gas flowing in is called the eluent, and the gas that is displaced from the solid and flows out is the eluate.

2.1. Tube Geometry

Figure 1 illustrates the geometry of the tube. It has an inside diameter *ID* that defines the width of the open channel through which gas flows, and an outside diameter *OD* that is equal to *ID* plus twice the wall thickness. The tube length is *L*. Typical values used in analytical gas chromatography columns from vendors such as Phenomenex, Supelco, or Restek are 0.1 to 0.5 mm *ID*, 5 to 30 m *L*, and wall thickness 0.1 to 10 micrometers. Thicker walls are desirable for a preparative-scale isotope separation system. Palladium tubing 0.8 mm *ID*, 0.2 m *L*, and 0.1 mm wall thickness is a catalog item sold by Goodfellow.

Figure 1. Geometry of open tube with inner surface of tube coated with metal hydride. Tube is typically much longer vs. its diameter than illustrated here.

A distance along the length of the tube is denoted by *z*, and along the radius of the tube by *r*. In some cases, it is convenient to refer to the inside radius $r_o = ID/2$. Other important values are the surface area of the wall per unit length *S*, which is the same as the circumference of the cross section of the gas channel; and the volumes of the gas and solid phases per unit length, A_g and A_s, which are the same as the corresponding areas of the cross section.

$$S = \pi \cdot ID = 2\pi r_0 \tag{1}$$

$$A_g = \frac{\pi}{4} ID^2 = \pi r_0^2 \tag{2}$$

$$A_s = \frac{\pi}{4}\left(OD^2 - ID^2\right) \tag{3}$$

2.2. Properties of gas and solid phases

2.2.1. Gas molecules

In this work, it is helpful to dodge the complications associated with the fact that gas-phase hydrogen is diatomic. However, it is valuable to predict the concentrations of the diatomic species, including mixed-isotope species such as HD. The differential equations presented in this report will account for gas-phase hydrogen by atoms. The concentrations of the diatomic species can be calculated in a post-processing step once the atom concentrations are known, with the assumption that the diatomic species are always at chemical equilibrium with each other.

This work builds on the assumption that the temperature T is constant, and the pressure drop across the tube is small, so the pressure P and concentration C_g of the gas atoms can be taken as constant, according to the ideal gas law, $C_g = 2P/R_gT$, R_g being the ideal gas constant. C_g is about 82 mM at room temperature and pressure. It is also assumed that no gas properties such as viscosity, diffusion constant, or molecular speed are isotope- or composition-dependent.

When determining the concentrations of diatomic species, the enthalpy of formation of the mixed-isotope species is assumed to be zero. In that case, the atoms combine as if they were drawn out of a hat in pairs. If the hat contains equal numbers of H and D atoms, two combinations form the single mixed-isotope species that can be denoted DH or HD, and one each form H_2 and D_2, so their ratio will be 2:1:1. More generally, the diatomic gases will obey the equilibrium relationship

$$K_{\mathrm{HD}} = \frac{[\mathrm{HD}]^2}{[\mathrm{H_2}][\mathrm{D_2}]} = 4 \tag{4}$$

where the brackets indicate the concentration of each species, and K_{HD} is the equilibrium constant. This corresponds to the chemical reaction

$$\mathrm{H_2} + \mathrm{D_2} \Leftrightarrow 2\mathrm{HD} \tag{5}$$

If H is the concentration of gas-phase hydrogen atoms, with the number of deuterium atoms being the difference between this and C_g, the diatomic species can be calculated by summing the number of each type of atom in each diatomic species, and incorporating the equilibrium expression.

$$[\mathrm{H_2}] = \frac{H - [\mathrm{HD}]}{2} = \frac{H^2}{2C_g} \tag{6}$$

$$[\mathrm{D_2}] = \frac{C_g - H - [\mathrm{HD}]}{2} = \frac{(C_g - H)^2}{2C_g} \tag{7}$$

$$[\mathrm{HD}] = H\left(1 - \frac{H}{C_g}\right) \tag{8}$$

These diatomic species expressions sum to $C_g/2$, the total concentration of diatomic molecules in the gas phase. For the remainder of this report, *H* will be used to denote the eluent gas atoms, and HD to denote the mixed-isotope diatomic gas, although no assumptions are made that are specific to these isotopes. Any reference to eluate atoms as "D" will be without italics to avoid confusion with diffusion constants.

In the real world, there is a small enthalpy of formation of HD, which causes K_{HD} to be slightly less than 4, and temperature-dependent.[2] This leads to the more complicated formula

$$[\mathrm{HD}] = C_g \frac{\left[1 + 4\left(\frac{4}{K_{\mathrm{HD}}} - 1\right)\frac{H}{C_g}\left(1 - \frac{H}{C_g}\right)\right]^{1/2} - 1}{\left(\frac{4}{K_{\mathrm{HD}}} - 1\right)} \tag{9}$$

which can be used to derive the other diatomic gas concentrations. The simpler expression will be used for the remainder of this work.

2.2.2. Solid phase

The total concentration of hydrogen isotopes in the solid phase is assumed to be a constant, C_s, with the eluent isotope denoted by H_s and the eluate by $\mathrm{D}_s = C_s - H_s$. In palladium hydride at room temperature under 1 atm H_2, C_s is about 70 M. Known variations with temperature, pressure, and isotopic composition are usually within about 10 percent, as long as the gas pressure is maintained above the transition to the dehydrided state.

Diffusion constants D_s of hydride species within a solid phase are much lower than those of gas-phase species. 5×10^{-8} cm^2/s is a typical value at room temperature, which is about 100 times lower than that for a dye molecule in water.[12]

2.3. Chemical reaction

The hydrogen-deuterium exchange reaction has been formulated previously by Foltz and Melius using diatomic gas-phase species,[2] but it is simpler to consider in monatomic form. It can be written as

$$\mathrm{H} + \mathrm{D}_s \Leftrightarrow \mathrm{H}_s + \mathrm{D} \tag{10}$$

where the subscript indicates an atom in the solid hydride phase, and no subscript indicates an atom in the gas phase. The equilibrium constant, also known in this context as the separation factor, is

$$\alpha = \frac{H_s \cdot \mathrm{D}}{H \cdot \mathrm{D}_s} \tag{11}$$

for concentrations measured at equilibrium.[13,14] It reflects whether the eluent or eluate is more stable in the solid phase; it is greater than 1 in the former case. If the reaction is not at equilibrium, as is sometimes assumed in this report, it will approach equilibrium at a finite rate. The net reaction rate R is the forward reaction rate minus the reverse reaction rate:

$$R = \alpha k \frac{H}{C_g}\left(1 - \frac{H_s}{C_s}\right) - k \frac{H_s}{C_s}\left(1 - \frac{H}{C_g}\right) \tag{12}$$

If k is a rate constant in mol/cm^2 s, R is a flux of H from the gas into the solid. The rate law states that a reaction occurs if a gas atom collides with a solid-phase hydrogen atom at the surface with the necessary configuration to cause a displacement reaction (as reflected by k) multiplied by the probability that the pair is the right isotopic combination for a forward or reverse reaction. The reaction is at equilibrium when $R = 0$; the equilibrium constant can be derived from this case. The net reaction rate can be rewritten as

$$R = \alpha k \frac{H}{C_g} - k \frac{H_s}{C_s} + (1 - \alpha) k \frac{H \cdot H_s}{C_g \cdot C_s} \tag{13}$$

showing that the nonlinear term cancels when $\alpha = 1$. A first-order equilibrium constant K can then be written as

$$K = \frac{H_s}{H} = \alpha \frac{C_s}{C_g} \tag{14}$$

where α is retained in case a first-order approximation can be found useful when α is nearly, but not exactly, 1.

Because α is a thermodynamic property, there is an ambiguity in how α connects to the net reaction rate. As α increases, either the forward reaction gets faster, or the reverse reaction gets slower, or a combination of these. In ion-exchange chromatography, increasing α has customarily been interpreted as a slowing reverse reaction, whereas here it is interpreted as a hastening forward reaction. Foltz and Melius considered a combination of both by including $\sqrt{\alpha}$ in each term. The choice can affect how a model scales with α and k.

Determining the change per unit time of concentration in each phase caused by the reaction requires multiplication of the flux R by the surface area per unit length S to get the molecules per

unit length per unit time crossing the boundary between phases, then dividing by the volume per unit length A_s or A_g to obtain concentrations. In the absence of any other transport phenomena such as advection (flow) or diffusion, this means

$$\frac{dH_s}{dt} = R\frac{S}{A_s} \tag{15}$$

$$\frac{dH}{dt} = -R\frac{S}{A_g} \tag{16}$$

A crude estimate of k can be made by constructing a flux of gas atoms that are attempting to react at the surface, and multiplying by a probability that the reaction is successful. The gas atoms move at a mean speed v_m, and the product of this and the gas concentration gives the rate of atomic impingement of a surface, if a factor of 1/4 is included to account for the fact that the atoms are moving in all directions, and not all are traveling toward the surface at a given time.[15] The mean speed is given by

$$v_m = \sqrt{\frac{8R_gT}{\pi M}} \tag{17}$$

where M is the mass of one mole of gas molecules. For H_2 at room temperature and pressure, v_m is about 1777 m/s, yielding an atomic impingement rate of about 3.6 mol H/cm^2 s. The reaction probability can be much less than 1 by various mechanisms, including an activation barrier to the reaction. At room temperature, an activation barrier E_a of 25 kJ/mol H decreases the reaction probability by more than 10^4. This motivates definition of a rate constant v_k with units of velocity:

$$v_k = \frac{k}{C_g} = \frac{v_m}{4}\exp\left(\frac{-E_a}{R_gT}\right) \tag{18}$$

2.4. Gas transport

The gas velocity can be treated at several levels of detail. In some cases, the velocity can be assumed to be uniform across the cross-section of the tube. This allows for a one-dimensional model of the tube. More sophisticated versions, such as that used by Golay, include Poiseuille's parabolic velocity profile for laminar fluid flow in a pipe

$$v(r) = 2v_0\left(1-\frac{r^2}{r_0^2}\right) \tag{19}$$

where v_0 is the radially averaged gas velocity. The symbol v_0 is also used here to describe the gas velocity in the one-dimensional case. The pressure drop associated with Poiseuille flow is given by

$$\frac{dP}{dx} = -\frac{8\pi\mu v_0}{A_g} \tag{20}$$

where μ is the gas viscosity, about 10^{-5} Pa s for H_2.[16] If the velocity is constant, this implies

$$\frac{\Delta P}{P} = \frac{8\pi\mu v_0 L}{0.5 C_g A_g R_g T} \tag{21}$$

The factor of 0.5 in the denominator reflects the fact that C_g is a monatomic gas concentration, whereas pressure is determined by a diatomic gas concentration. If this pressure ratio is not much less than 1, it is advisable to account for decreases of C_g and increases in v_0 along the length of the tube. The product $0.5 C_g A_g v_0$ is the diatomic molar flow rate $\dot{n}$ through the tube. If this is considered constant, integration of the flow equation gives the axial dependence of C_g and v_0.

$$\frac{C_g(z)}{C_g(L)} = \frac{v_0(L)}{v_0(z)} = \left[\frac{64\pi\mu\dot{n}(L-z)}{R_g T\left(A_g C_g(L)\right)^2} + 1\right]^{1/2} = \left[\frac{16\pi\mu(L-z)v_0^2(L)}{\dot{n}R_g T} + 1\right]^{1/2} \tag{22}$$

Either square root expression could be used, depending on whether it is more convenient to specify the concentration or the velocity at the exit. This axial variation will be considered only briefly in this report.

The diffusion constants D of all gas-phase species are assumed to be the same. A reasonable value for diatomic hydrogen at room temperature and pressure is 1 cm^2/s.[17] Gas-phase diffusion constants are inversely proportional to pressure or concentration.

3. GAS CHROMATOGRAPHY: FIRST-ORDER REACTION

In this chapter, models of open-tube gas chromatography are described, assuming a first-order chemical reaction between the gas and solid phase, with increasingly detailed descriptions of mass transport effects. These include the approach of Golay, along with some extensions, and approaches to optimization. These models will be useful for comparison to (and in some cases are applicable to) the case of the second-order reaction.

3.1. Combination of equilibrium reaction and mass transport

3.1.1. Flow plus reaction

In the simplest case considered here, the chemical reaction is assumed to be at equilibrium everywhere in the tube, and gas flows through, without diffusing. With no radial concentration gradient, the problem can be treated in one dimension. A mass balance equation provides that the rate of increase in H at a given axial position is sum of the difference between the amounts flowing in and out within the gas phase (given by the first term) and the amount that enters from the solid phase, which is given by the second term, assuming that the amount leaving the solid phase equals the amount entering the gas phase.

$$\frac{\partial H}{\partial t} = -v_0 \frac{\partial H}{\partial z} - \frac{A_s}{A_g} \frac{\partial H_s}{\partial t} \tag{23}$$

As boundary conditions, H and H_s are zero everywhere at $t = 0$. At all later times, $H = C_g$ at the inlet. For fast reaction kinetics, the reaction is always at equilibrium, and H_s can be eliminated by using the equilibrium constant:

$$\frac{\partial H}{\partial t} = -v_0 \frac{\partial H}{\partial z} - \alpha k' \frac{\partial H}{\partial t} \tag{24}$$

where

$$k' = \frac{C_s A_s}{C_g A_g} \tag{25}$$

which is the ratio of capacity of material in the solid phase to capacity of material in the gas phase. Golay and others lump α into k', but it will help clarify the nonlinear case if this is not done here. The mass balance equation simplifies to

$$\frac{\partial H}{\partial t} = -\frac{v_0}{1+\alpha k'} \frac{\partial H}{\partial z} \tag{26}$$

With the boundary conditions given, H is a step function at $z = 0$ just after $t = 0$. The mass balance equation moves the function H along the tube with the reduced velocity defined by the coefficient.
In the real world, the initial step would not be infinitely sharp. This equation predicts that the sharpness is preserved. For example, if the initial distribution looks like an error function, the solution would look like

$$\frac{H}{C_g} = \frac{1}{2} - \frac{1}{2}\,\mathrm{erf}\left(\frac{x - \left(v/\left(1+k'\right)\right)t}{\sigma}\right) \tag{27}$$

where σ is a parameter that determines the width of the initial distribution. This solution has a concentration boundary that moves at the reduced velocity, but does not broaden with time. The concentration boundary is also known as the reaction front, because when σ is small, it is a localized region where R is high. Figure 2 shows the resulting diatomic gas concentrations that elute from the end of the tube. The reaction front traverses a column of length L in the elution time

$$t_{el} = \left(1 + \alpha k'\right)\frac{L}{v_0} \tag{28}$$

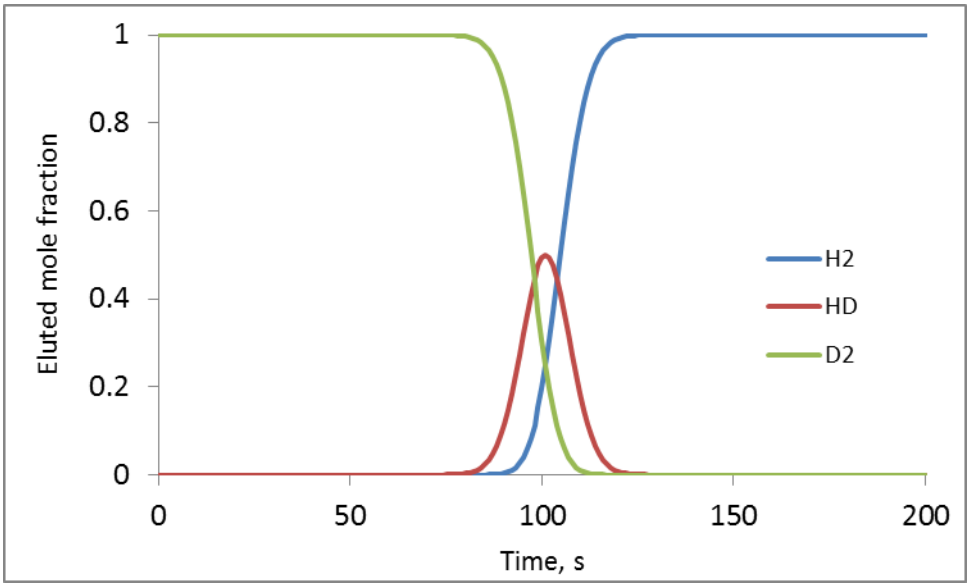

Figure 2. Eluted mole fractions versus time as predicted by error function expression for $\alpha = 1$, $k' = 100$, $L/v_0 = 1$ s, $\sigma = 0.1$.

3.1.2. Flow plus reaction plus axial diffusion

The mass balance can be modified by including a diffusion term that allows gas to spread along the length of the tube, and soften sharp concentration gradients.

$$\frac{\partial H}{\partial t} = D\frac{\partial^2 H}{\partial z^2} - v_0 \frac{\partial H}{\partial z} - \frac{A_s}{A_g}\frac{\partial H_s}{\partial t} \tag{29}$$

At the outlet, the axial diffusion term is omitted from the equation, so no information is needed from points downstream; the diffusion-free mass balance acts as the boundary condition. Incorporating reaction equilibrium leads to

$$\frac{\partial H}{\partial t} = \frac{D}{1+\alpha k'}\frac{\partial^2 H}{\partial z^2} - \frac{v_0}{1+\alpha k'}\frac{\partial H}{\partial z} \tag{30}$$

so diffusion is reduced similarly to the velocity. For a sharp initial step, this has the closed-form solution

$$\frac{H}{C_g} = \frac{1}{2} - \frac{1}{2} erf\left(\frac{x - \left(v_0/\left(1+\alpha k'\right)\right)t}{\sqrt{4\left(D/\left(1+\alpha k'\right)\right)t}}\right) \tag{31}$$

This function has a reaction front that moves at the reduced velocity, and broadens at the reduced diffusion constant. Substitution of t_{el} here gives the form of the function at that time:

$$\frac{H}{C_g} = \frac{1}{2} - \frac{1}{2} erf\left(\frac{x - L}{\sqrt{4DL/v_0}}\right) \tag{32}$$

This shows that the diffusive broadening in a column of a given length is independent of *k'*, but it does depend on the gas velocity: a slower velocity gives the gas more time to diffuse and broaden as it travels down the column.

3.1.3. Flow plus reaction plus axial and radial diffusion

Another broadening effect can be hypothesized where the gas concentration varies radially, and diffusion is the only mechanism to reduce this concentration gradient. Including a radial diffusion term yields

$$\frac{\partial H}{\partial t} = D\frac{\partial^2 H}{\partial z^2} + D\frac{1}{r}\frac{\partial}{\partial r}\left(r\frac{\partial H}{\partial r}\right) - v_0\frac{\partial H}{\partial z} \tag{33}$$

In this case, the relationship between H and H_s is accounted for by defining a flux at the boundary $r = r_0$ that satisfies the equilibrium condition.

$$-D\frac{\partial H}{\partial r} = \frac{A_s}{S}\frac{dH_s}{dt} = \alpha k'\frac{A_g}{S}\frac{dH}{dt} = \frac{\alpha k' r_0}{2}\frac{dH}{dt} \tag{34}$$

This equation is not known to have a closed-form solution. However, Golay chose to study a similar problem, and was able to gain a significant amount of insight.

3.1.4. Poiseuille flow, reaction, axial and radial diffusion (Golay's case)

Once the transition from the one-dimensional to the two-dimensional case has been made, it is straightforward to incorporate the radial dependence of the gas velocity, as follows.

$$\frac{\partial H}{\partial t} = D\frac{\partial^2 H}{\partial z^2} + D\frac{1}{r}\frac{\partial}{\partial r}\left(r\frac{\partial H}{\partial r}\right) - 2v_0\left(1-\frac{r^2}{r_0^2}\right)\frac{\partial H}{\partial z} \tag{35}$$

This is the case that Golay considered in detail by applying the method of moments, which postulates a peak-shaped solution (analogous to the HD peak) and derives properties of its area, position, and width. A key result of this is

$$\left(\frac{\sigma}{L}\right)^2 = \frac{1}{N} = \frac{2D}{v_0 L} + \frac{1+6\alpha k' + 11(\alpha k')^2}{(1+\alpha k')^2}\frac{v_0 r_0^2}{24DL} \tag{36}$$

where σ^2 is the second moment of the peak (a measure of its width), and N the number of theoretical plates, which is simply a name for this expression that invokes a connection to other theories of chemical separations such as distillation. N is a useful measure of the sharpness of the peak in comparison to the elution time. For large $\alpha k'$, and approximating 11/24 as 1/2, this approaches

$$\frac{1}{N} = \frac{2D}{v_0 L} + \frac{v_0 r_0^2}{2DL} \tag{37}$$

The first term captures the effect of axial diffusion, and is consistent with the observation made in the one-dimensional case. Ignoring factors of two, it is approximately the ratio of the time required for gas to blow through the column (regardless of species identity), given by L/v_0, to a characteristic time required to diffuse the length of the column, L^2/D. This term becomes important if the gas velocity is too slow, and is also known as the Peclet number. The second term captures the effect of radial diffusion. It is approximately the ratio of a characteristic time required for gas to diffuse radially, r_0^2/D, divided by the time required for gas to blow through the column. It contributes to broadening at high gas velocities, and especially at large r_0. Golay also considered a tube with a rectangular cross section, and obtained a different polynomial coefficient on the radial diffusion term. One might expect that a method of moments analysis of the case of radially uniform gas velocity would have a similar effect on the result.

3.1.5. Optimization in Golay's case

The fact that one broadening mechanism contributes at low velocities and another at high velocities suggests that there is a gas velocity where broadening is minimized:

$$v_{opt} = \frac{2D}{r_0} \tag{38}$$

At this velocity, the number of plates is equal to the aspect ratio of the tube:

$$N_{opt} = \frac{L}{2r_0} \tag{39}$$

Figure 3 shows the number of plates as a function of gas velocity for various tube diameters. At low gas velocities, the axial diffusion term governs the number of plates. No design parameters are available to adjust this region of the curve. Radial diffusion is strongly dependent on tube radius (or diameter), affecting the optimum and the number of plates at the optimum. Note that at numbers of plates below 10, the assumption made by Golay that $\sigma << L$ breaks down, but such values are included in the plot for illustrative purposes. The plate curves are modified if the chemical reaction deviates from equilibrium, as discussed in the next section.

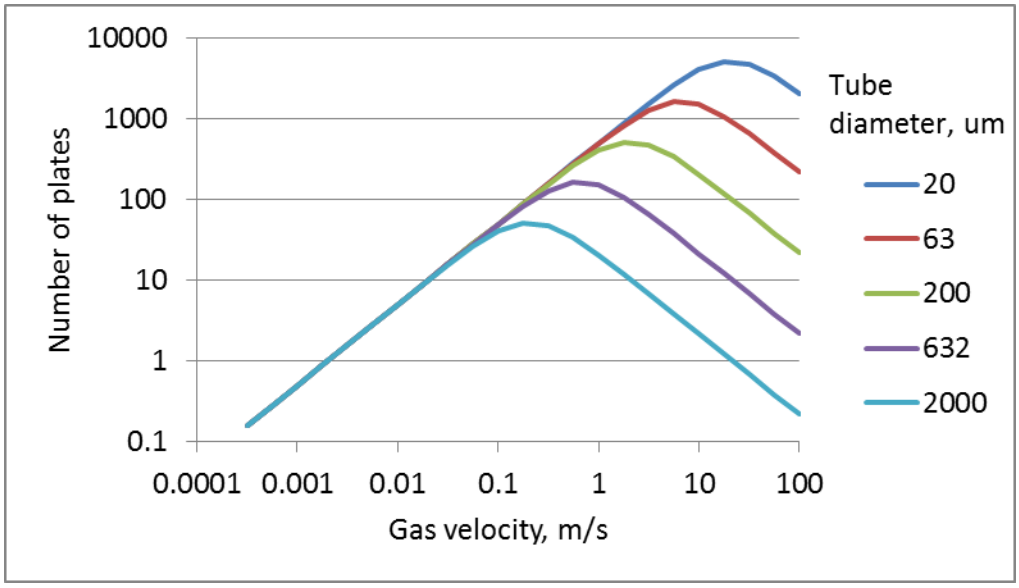

Figure 3. Number of plates versus gas velocity as predicted by Golay for several tube diameters, with D=10^{-4} m^2/s, α=1 and L=0.1 m.

For the maximum number of plates for the smallest diameter shown, the inlet pressure is about 10x the outlet pressure, so the assumption of constant velocity does not apply. That pressure difference decreases rapidly with diameter: $\Delta P/P$ is less than 50% for 63 um and less than 2% for the others.

3.2. Finite reaction rate

3.2.1. One-dimensional case

In one dimension, the kinetically limited case (neglecting all diffusion) for a first-order reaction can be described as

$$\frac{\partial H}{\partial t} = -v_0 \frac{\partial H}{\partial z} - \frac{A_s}{A_g}\frac{\partial H_s}{\partial t} \tag{40}$$

$$\frac{\partial H_s}{\partial t} = \frac{S}{A_s}\left(\alpha k \frac{H}{C_g} - k\frac{H_s}{C_s}\right) \tag{41}$$

A closed-form solution to the case of $\alpha = 1$ is known, but it is rather complicated, and introduced in the next chapter.

3.2.2. Two-dimensional case; Number of theoretical plates

While Golay restricted his attention to the case of rapid equilibration, Clifford more recently reported a version accounting for a finite rate of reaction.[18] The version presented here is modified to account for absorption into the metal hydride (and not just adsorption to a surface). The flux at the boundary is asserted to be equal to the rate of a finite, first-order net reaction rate. The rate law used is from the previous section, omitting the nonlinear term, but still relevant to that case if α is very close to 1.

$$-D\frac{\partial H}{\partial r} = \alpha k \frac{H}{C_g} - k\frac{H_s}{C_s} \tag{42}$$

The accumulation of H_s is also proportional to this reaction rate, with a coefficient that converts flux to a rate of concentration change in the solid phase:

$$\frac{\partial H_s}{\partial t} = \frac{S}{A_s}\left(\alpha k \frac{H}{C_g} - k\frac{H_s}{C_s}\right) \tag{43}$$

This leads to the following expression for the number of theoretical plates.[19]

$$\left(\frac{\sigma}{L}\right)^2 = \frac{1}{N} = \frac{2D}{v_0 L} + \frac{(\alpha k')^2}{(1+\alpha k')^2}\frac{v_0 r_0}{\alpha v_k L} + \frac{1+6\alpha k'+11(\alpha k')^2}{(1+\alpha k')^2}\frac{v_0 r_0^2}{24DL} \tag{44}$$

or approximately for $\alpha k' > 10$,

$$\left(\frac{\sigma}{L}\right)^2 = \frac{1}{N} = \frac{2D}{v_0 L} + \frac{v_0 r_0}{\alpha v_k L} + \frac{11 v_0 r_0^2}{24 D L} \tag{45}$$

Consideration of a finite reaction rate leads to an additional term in the theoretical plate expression that measures the contribution of slow kinetics to the broadening, which can be recognized as the reciprocal of a Damköhler number. Ignoring factors of two, it is the ratio of a characteristic time required for a tube full of the gas-phase hydrogen atoms to undergo reaction, $C_g A_g L / \alpha k S L$, to the time required for gas to blow through the tube, L/v_0. This term is of increasing importance at higher gas velocities. As before, there is a gas velocity that optimizes the number of plates for a given tube geometry by balancing axial diffusion with the other broadening mechanisms. As the tube gets longer, all three terms lead to increased broadening, but the broadening increases less than the increase in length, so use a longer column still leads to more plates.

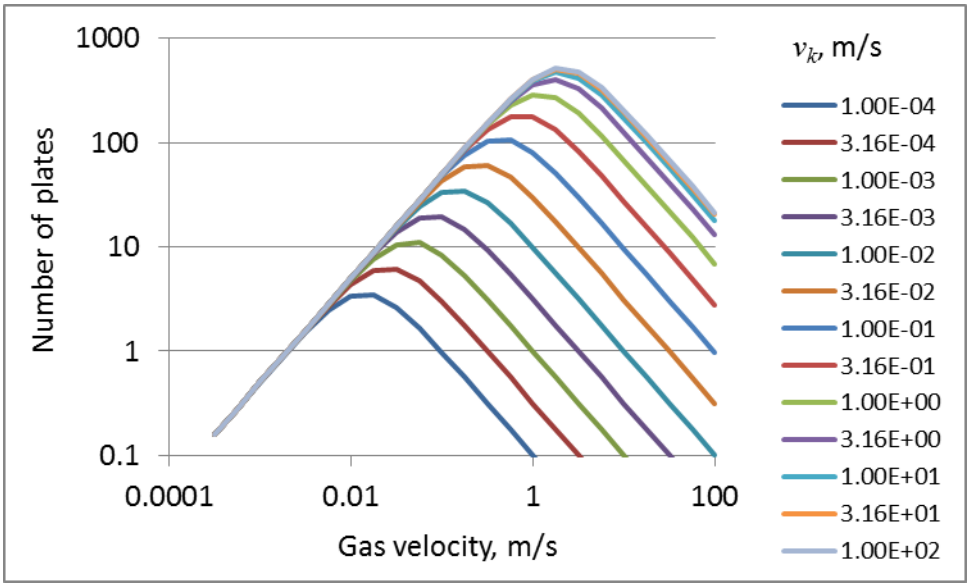

Figure 4. Number of plates versus gas velocity as predicted by Clifford for several reaction rate constants, with D=10^{-4} m^2/s, r_0=10^{-4} m, α=1 and L=0.1 m.

Figure 4 illustrates the effect of slow reaction kinetics on the optimum number of plates. For fast kinetics, the reaction rate is still limited by radial diffusion at high gas velocities, but in this example, once v_k < 3 m/s, the slow reaction limits the rate at high gas velocities, and decreases the optimum number of plates and optimum gas velocity. When kinetically limited, these values are

$$v_{opt} = \sqrt{\frac{2 D v_k}{r_0}} \tag{46}$$

At this velocity, the number of plates is:

$$N_{opt} = \frac{L}{2}\sqrt{\frac{v_k}{2Dr_0}} \tag{47}$$

3.2.3. Performance optimization

The hydride tube provides several adjustable design parameters that can be optimized toward a certain goal, given practical constraints. In an experimental context, the goal may be to maximize the contribution of kinetics to the number of theoretical plates, at the expense of the contributions from diffusion. The plate expression would suggest using higher velocities and narrower tubes.

For a practical chemical separation, maximizing the number of theoretical plates is not necessarily the most practical goal. For example, there is no need to produce an elution front that is much sharper than the response time of a detector or valve at the outlet. More desirable would be to choose an acceptable number of theoretical plates, and maximize the number of theoretical plates obtained per unit time at the elution time. A similar approach that minimizes "plate duration" (the time required to achieve a theoretical plate) has been described.[20] Clifford provides a version of the theoretical plate expression as a function of time. Manipulation of this reveals that the rate of plate production is maximized when the following expression is minimized:[21]

$$\frac{2D}{v_0^2} + \frac{r_0}{\alpha v_k} + \frac{r_0^2}{2D} \tag{48}$$

This suggests that the velocity should be maximized, and radius minimized. However, there is a limit on how long and narrow the tube can be, because both changes in geometry cause an increase in pressure drop. If $\Delta P/P$ is limited to 0.1, the tube radius can be constrained, changing this expression to

$$\frac{2D}{v_0^2} + \frac{1}{\alpha v_k}\left(\frac{160\mu L v_0}{C_g R_g T}\right)^{1/2} + \frac{80\mu L v_0}{D C_g R_g T} \tag{49}$$

The presence of velocity in both the numerator and denominator of various terms indicates that an optimal velocity exists, given the other parameters. L can be chosen to give the desired number of theoretical plates, with the pressure drop constraint:

$$\frac{1}{N} = \frac{v_0}{L}\left[\frac{2D}{v_0^2} + \frac{1}{\alpha v_k}\left(\frac{160\mu L v_0}{C_g R_g T}\right)^{1/2} + \frac{80\mu L v_0}{D C_g R_g T}\right] \tag{50}$$

Increasing L increases N but decreases its rate of production. The required r_0 can be obtained from the pressure drop formula. Figures 2-4 show values of these criteria for the parameter values described in Table 1. There is not a single, practical optimum for both v_0 and L, but some choices are clearly better than others, and a designer retains some freedom to choose values appropriate for a specific scenario. In the example shown here, tube lengths of at least 1 m are needed to obtain 1000 theoretical plates, but unnecessary length makes the process unnecessarily slow. The gas velocity giving the optimum number of plates per unit time is about 1 m/s, although the number of plates is maximized at about half of this velocity. The radius under these conditions is in the high tens of micrometers.

Table 1. Parameters used in Figures 5-7.

Parameter	Value	Units
D	10^{-4}	m^2/s
μ	$9x10^{-6}$	Pa s
v_k	10^{-1}	m/s
$C_q R_q T$	$2x10^5$	Pa

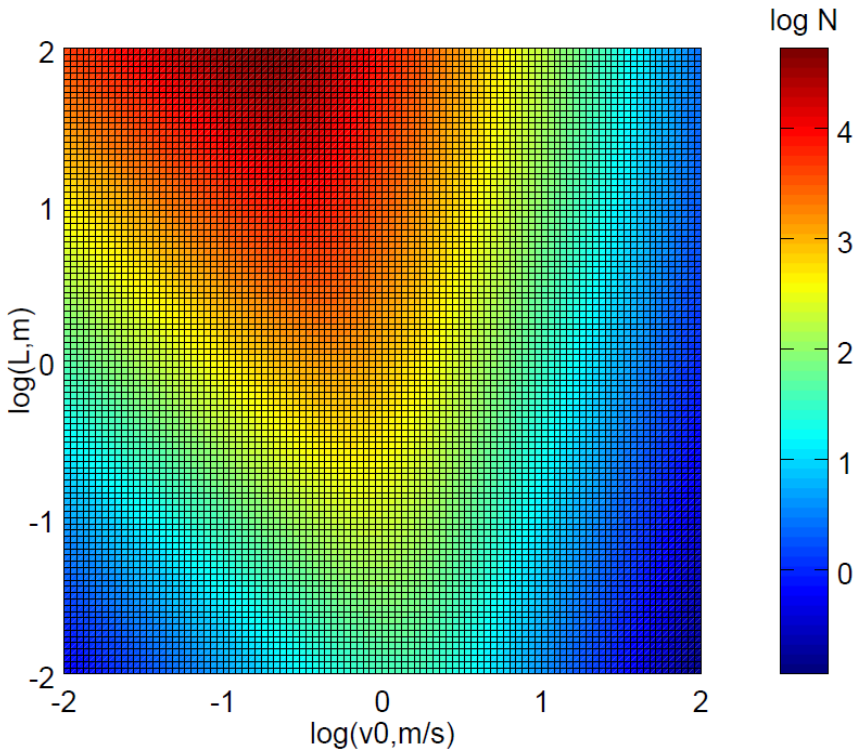

Figure 5. Number of theoretical plates as a function of gas velocity and tube length for the parameters in Table 1.

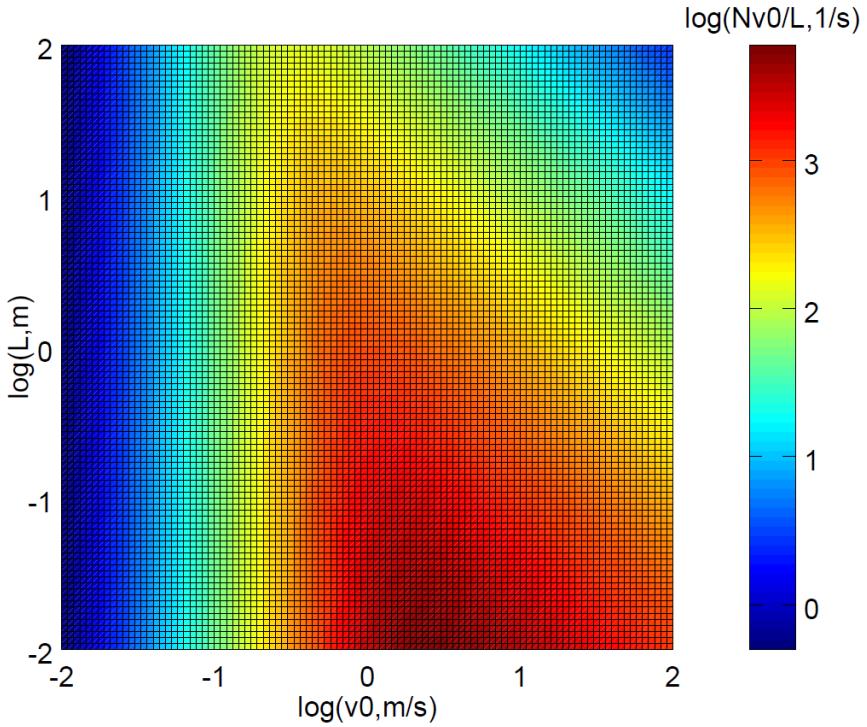

Figure 6. Nv_0/L as a function of gas velocity and tube length for the parameters in Table 1.

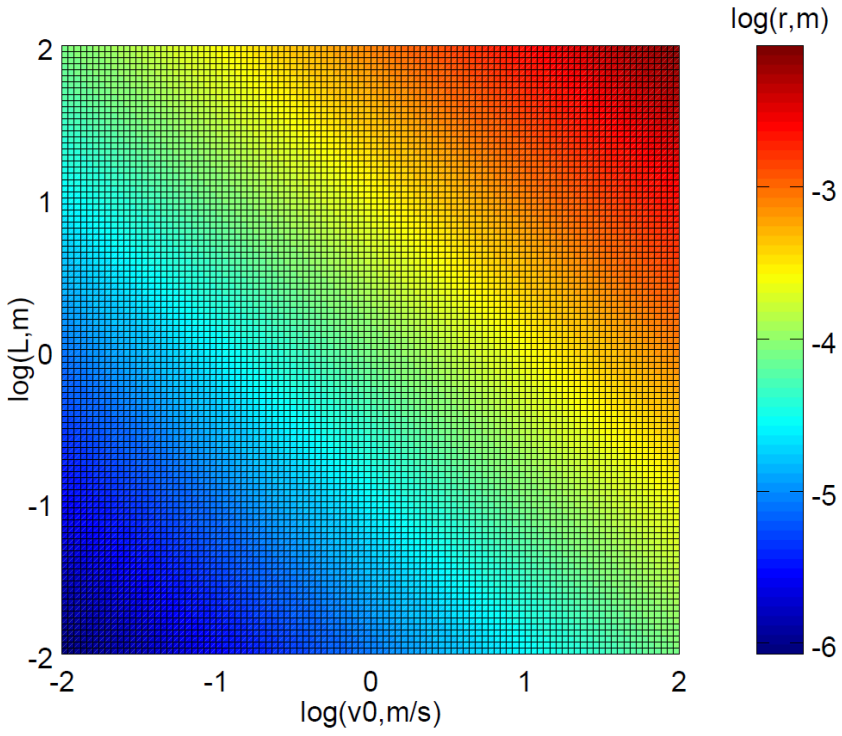

Figure 7. Tube radius as a function of gas velocity and tube length for the parameters shown in Table 1.

4. GAS CHROMATOGRAPHY: SECOND-ORDER REACTION

4.1. Properties of the solution

Walter examined the chromatography problem for the case of a second-order exchange reaction. He assumed rapid equilibrium between phases,[22] and the case of slow kinetics,[23] but did not consider diffusion. He assumed large *k'*, and treated the solid phase as a surface phase. The version presented here follows his argument, but uses a bulk solid phase, does not restrict *k'*, and uses the notation from the previous sections. Starting from the 1D mass balance without diffusion:

$$\frac{\partial H}{\partial t} = -v_0 \frac{\partial H}{\partial z} - \frac{A_s}{A_g} \frac{\partial H_s}{\partial t} \tag{51}$$

H_s is eliminated using the exchange equilibrium constant expression in Section 2.3, noting that D = C_g - H.

$$H_s = \frac{\alpha C_s H}{C_g + (\alpha - 1)H} \tag{52}$$

When $\alpha > 1$, this looks like a Langmuir isotherm with an initial slope equal to $\alpha C_s / C_g$, but saturating at $\alpha C_s / (\alpha - 1)$. This saturation is never reached, because H_s cannot exceed C_s, but this defines the curvature. Langmuir isotherms are considered frequently throughout the chromatography literature, and insight from that work can often be (cautiously) applied to this case. When $\alpha < 1$, this function has a positive curvature, and when $\alpha = 1$, it is a straight line. This is shown in Figure 8. The further significance of these functional forms will be discussed below. The isotherm can also be solved for H, which is sometimes a useful form:

$$H = \frac{C_g H_s}{\alpha(C_s - H_s) + H_s} \tag{53}$$

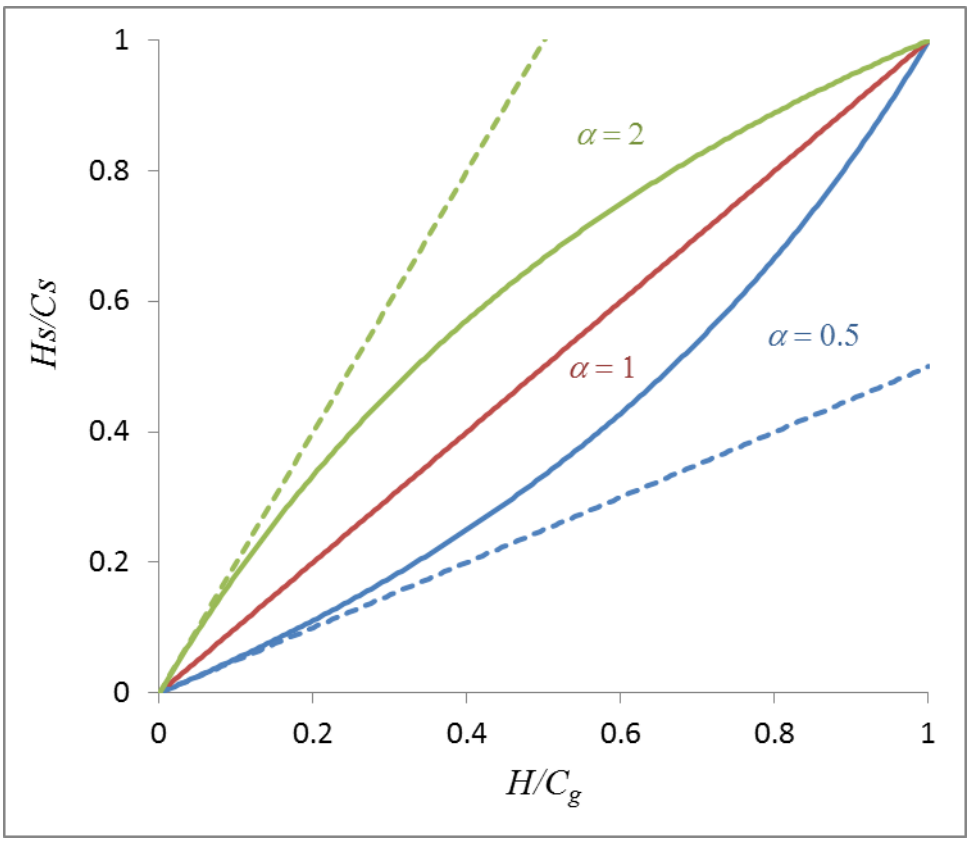

Figure 8. Relationship between H and H_s for several values of α. The dashed lines show the relationship for first-order reaction kinetics.

Proceeding with the elimination of H_s:

$$\frac{\partial H_s}{\partial t} = \frac{\alpha C_s}{C_g\left(1+(\alpha-1)(H/C_g)\right)^2}\frac{\partial H}{\partial t} \tag{54}$$

leading to

$$\left[1+\frac{\alpha k'}{\left(1+(\alpha-1)(H/C_g)\right)^2}\right]\frac{\partial H}{\partial t} = -v_0\frac{\partial H}{\partial z} \tag{55}$$

When $\alpha = 1$, this equation reduces to a form that appears in the previous section. Walter invokes the method of characteristics, which provides a form for the solution

$$H = f\left(\left[1+\frac{\alpha k'}{\left(1+(\alpha-1)(H/C_g)\right)^2}\right]z - v_0 t\right) \tag{56}$$

where f is an arbitrary function. The inlet boundary condition prescribes $H = C_g$ for negative values of the argument, which is true when

$$z < \frac{v_0}{1+k'/\alpha}t \tag{57}$$

Likewise, the initial condition prescribes $H = 0$ for positive values of the argument, which is true when

$$z > \frac{v_0}{1+\alpha k'}t \tag{58}$$

Between these values of z, the argument is zero, and this can be solved for H.

$$\frac{H}{C_g} = \frac{1}{1-\alpha}\left[1-\left(\frac{1}{\alpha k'}\left(\frac{v_0 t}{z}-1\right)\right)^{-1/2}\right] \tag{59}$$

Substitution in the equilibrium constant expression yields H_s:

$$\frac{H_s}{C_s} = \frac{\alpha}{1-\alpha}\left[\left(\frac{1}{\alpha k'}\left(\frac{v_0 t}{z}-1\right)\right)^{1/2}-1\right] \tag{60}$$

The valid range of z is only finite if $\alpha < 1$, as is the case when deuterium elutes hydrogen from a tube (though in this report, the eluent is always labeled "H" and the eluate always labeled "D").

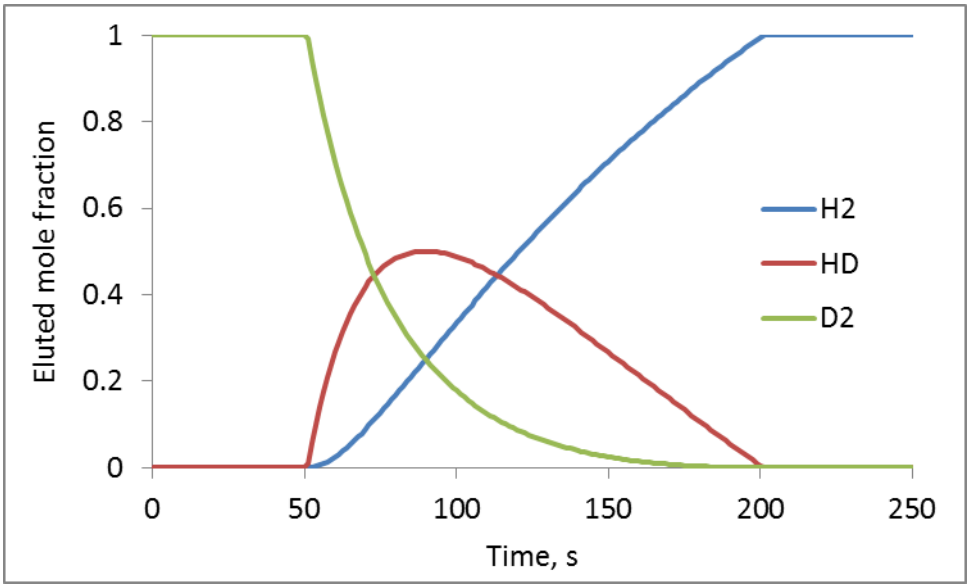

Figure 9. Eluted mole fractions versus time as predicted by Walter for α=0.5, k'=100, L/v_0=1 s.

Figure 9 shows that the HD peak is broad when $\alpha < 1$, even if the transport and reaction rates are fast. This result, and the case of larger α, can be understood by inspection of the differential equation that defines this model. At high z, where H is near zero, the equation looks like the linear form. At low z, where H is near C_g, α appears elsewhere in the reduced velocity.

$$\frac{\partial H}{\partial t} = -\frac{v_0}{1+\alpha k'}\frac{\partial H}{\partial z} \qquad \text{(high } z\text{)} \tag{61}$$

$$\frac{\partial H}{\partial t} = -\frac{v_0}{1+k'/\alpha}\frac{\partial H}{\partial z} \qquad \text{(low } z\text{)} \tag{62}$$

When $\alpha < 1$, the leading edge of the elution front moves faster than the trailing edge, causing the front to broaden. For $\alpha > 1$, assuming an elution front that starts out with a finite width, the trailing edge moves faster than the leading edge. With no other broadening mechanisms, the front gets compressed to infinite sharpness.

For the $\alpha > 1$ case, the reaction is exothermic. The H has a strong thermodynamic driving force to go into the solid, but is limited by how much D is around in the solid to be displaced. The gas at the leading edge easily finds D to displace, so the gas goes into the solid rather than moving forward. The gas at the trailing edge does not easily find D to exchange with, so it keeps moving forward down the column. However, when the reaction is endothermic ($\alpha < 1$), the material in the solid is being diluted (or soaked) out, which works best when there is more H around in the gas phase. At the leading edge, there is not much H, so not much D gets diluted into it, and the H keeps moving down the tube. At the trailing edge, more D comes out to be diluted by the larger amount of H, so there is less H to move down the tube. When there is no enthalpic driving force and $\alpha = 1$, these effects balance, and the front velocity is the same everywhere.

4.2. Solution for finite kinetics

A more complete analytical solution has been derived by Thomas for the case where exchange is kinetically limited.[24] This is the case governed by the 1D flow plus reaction equation, and the full expression for the time rate of change of H_s given in chapter 2. Thomas was studying the case of ion exchange in a packed zeolite column, but the derived solution can be adopted to hydrogen isotope exchange in a tube by identifying analogous parameters. This results in a function that requires several steps to be evaluated.

$$j_1 = (1/k')\frac{v_k S}{v_0 A_g}(v_0 t - z) \tag{63}$$

$$j_2 = \frac{v_k S}{v_0 A_g} z \tag{64}$$

$$\varphi(u_1, u_2) = \int_0^1 u_1 \exp(u_1(1-u_3)) I_0\left(2\sqrt{u_1 u_2 u_3}\right) du_3 \tag{65}$$

$$\frac{H}{C_g} = \frac{I_0\left(2\sqrt{\alpha j_1 j_2}\right) + \varphi(\alpha j_1, j_2)}{I_0\left(2\sqrt{\alpha j_1 j_2}\right) + \varphi(\alpha j_1, j_2) + \varphi(\alpha j_2, j_1)} \tag{66}$$

$$\frac{H_s}{C_g} = \frac{\varphi(\alpha j_2, j_1)}{I_0\left(2\sqrt{\alpha j_1 j_2}\right) + \varphi(\alpha j_1, j_2) + \varphi(\alpha j_2, j_1)} \tag{67}$$

where I_0 is the zero-order modified Bessel function of the first kind. The u's, j's, and φ are intermediate values in the calculation. If the coefficient on j_2 is interpreted as the reciprocal of a height equivalent to a theoretical plate, then j_2 is a measure of axial position in the column measured as a number of plates. The other intermediate parameters are of less enlightening physical significance; in the author's opinion, it is best to consider H and H_s as functions of z and t, along with parameters such as α and k'. The solution can be impractical to use for extremely large values of α, j_1, or j_2, because the Bessel function resembles an exponential function, leading to values large enough to be difficult to compute. However, it still captures a wide range of behavior for any realistic value of α, and includes the transient curve shapes at short times. However, the solution is undefined at times shorter than that needed for the gas to travel from the inlet to a given z. Figure 10 shows the HD peak shape predicted by Thomas under the same conditions as Figure 9, starting with the fastest kinetics predictable by the implementation of the Bessel function found in software such as Excel and Octave; large v_k values lead to large Bessel function arguments. The other curves have decreasing v_k by factors of 3. The fastest value closely resembles Figure 9, but with rounded corners at the beginning and end of the curve. The slower values lead to increased broadening.

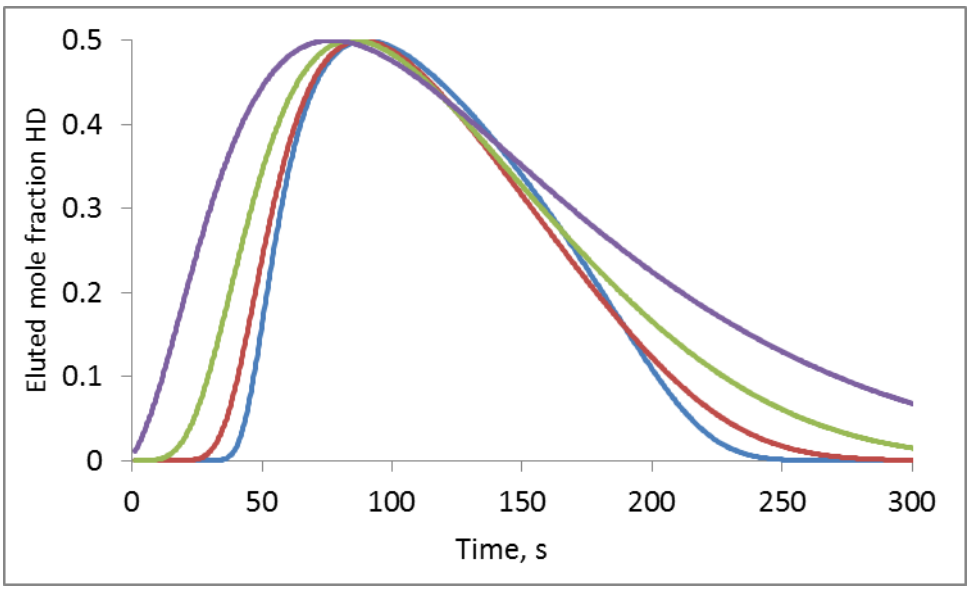

Figure 10. Eluted HD mole fractions versus time as predicted by Thomas for $\alpha = 0.5$, $k' = 100$, $L/v_0 = 1$ s, $v_k S/A_g = 280$ s^{-1} for the sharpest curve, decreasing by factors of 3.

As can also be predicted from Walter's formula, the curve broadens as the column length increases, as shown in Figure 11. When $\alpha = 1$, the HD peak becomes more symmetric, but still broadens with time, as is expected from the theoretical plate analysis in the previous chapter. However, when $\alpha > 1$, the curve does not broaden with time, and is sharper than the cases of lower α. A faster kinetic parameter was used for $\alpha = 0.5$ in order to keep the curves on scale; a lower value leads to broader peaks.

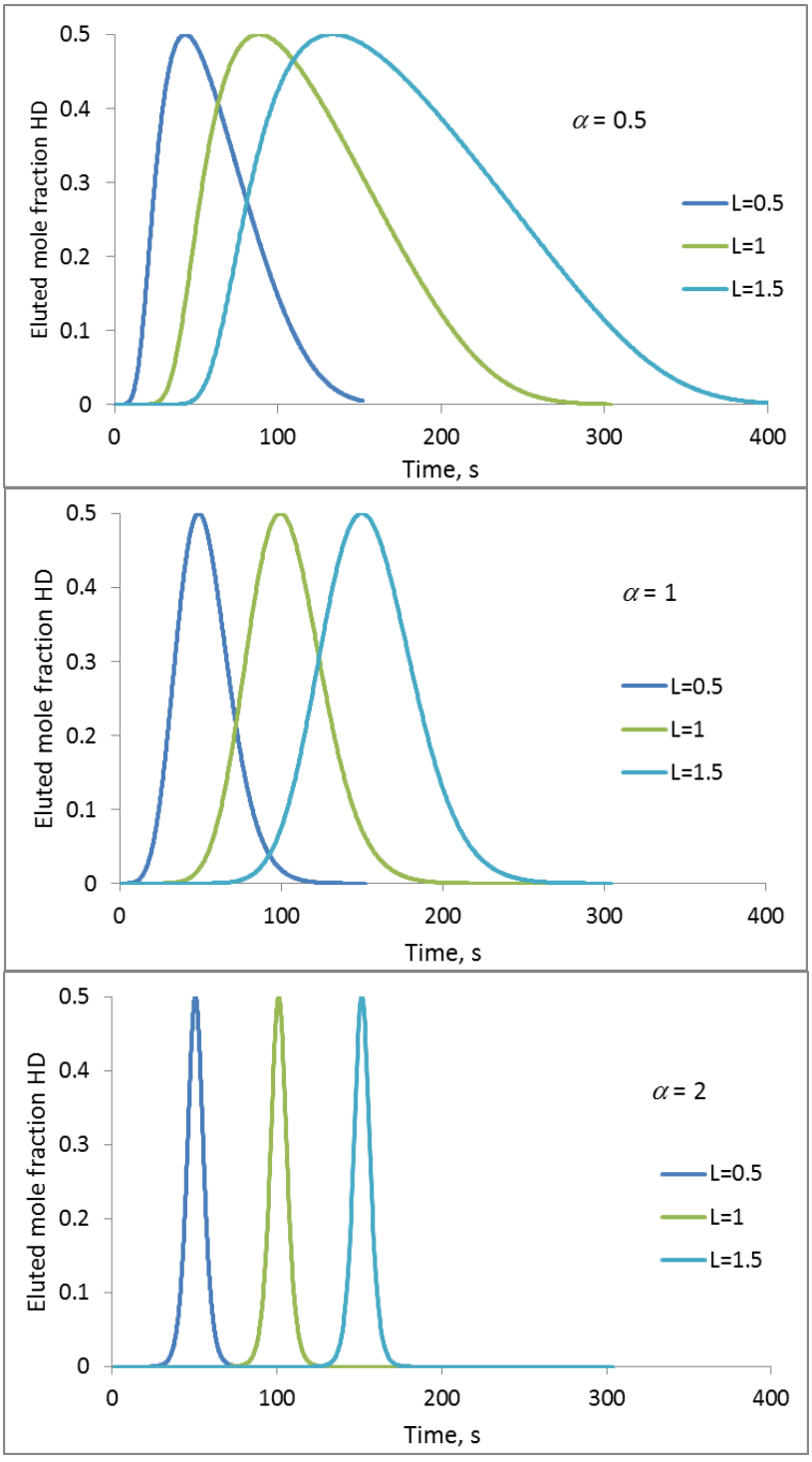

Figure 11. Eluted HD mole fractions versus time as predicted by Thomas for k' = 100, L/v_0 = 1 s, $v_k S/A_g$ = 93 s^{-1} for various tube lengths. Top: α = 0.5, $v_k S/A_g$ = 93 s^{-1}; middle: α = 1, $v_k S/A_g$ = 31 s^{-1}; bottom: α = 2, $v_k S/A_g$ = 31 s^{-1}.

When α is above 1, a balance is seen between kinetic broadening and thermodynamic narrowing of the peak. A simple limiting form can be obtained for α sufficiently above 1, and t sufficiently above zero:

$$\frac{H}{C_g} = \frac{1}{1+\exp\left[\dfrac{2v_k(\alpha-1)(1+k')}{k'v_0 r_0}\left(z-\dfrac{v_0}{(1+k')}t\right)\right]} \tag{68}$$

or equivalently

$$\frac{H}{C_g} = \frac{1}{2}+\frac{1}{2}\tanh\left(\frac{v_k(\alpha-1)(1+k')}{k'v_0 r_0}\left(z-\frac{v_0}{(1+k')}t\right)\right) \tag{69}$$

This function captures the competition between kinetic broadening, which scales with $1/v_k$, and thermodynamic sharpening, which scales with $\alpha-1$. The curve has a sigmoidal shape: that of the hyperbolic tangent, which is slightly different from the error function, as shown in Figure 12. There is apparently no simplified form of the solution derived by Thomas for the case of $\alpha = 1$, but its full form can be used. Because the nonlinear term in the rate law vanishes when $\alpha = 1$, Thomas's solution provides a connection to the first-order reaction described in the previous chapter.

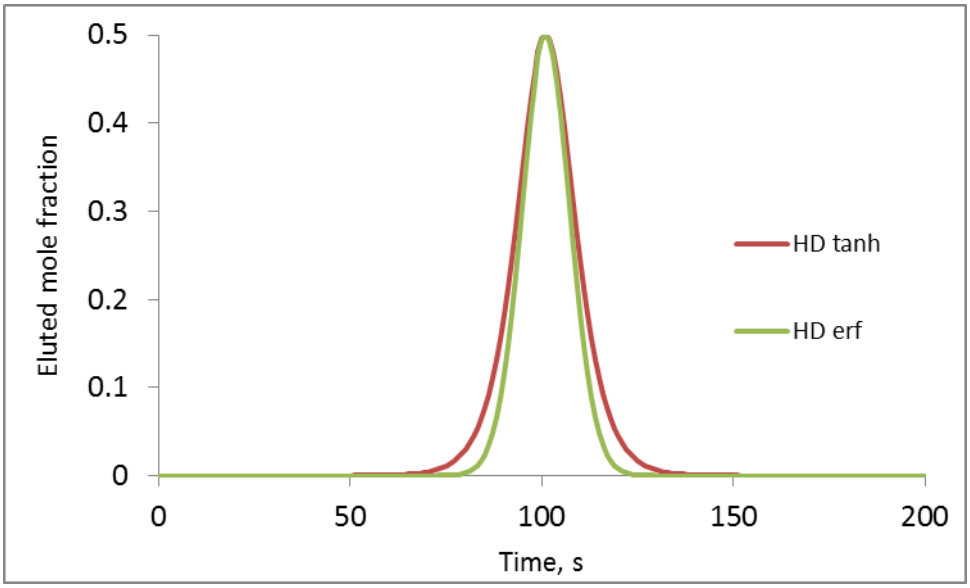

Figure 12. Eluted HD mole fractions versus time as predicted using an error function or hyperbolic tangent function to describe H/C_g under conditions equivalent to Figure 2.

The Thomas function captures the approach to this steady state, which occurs most slowly when α is only slightly above 1. In Figure 13, the steady-state condition is reached when the upstream tail of the HD peak is sufficiently far from the inlet of the tube.

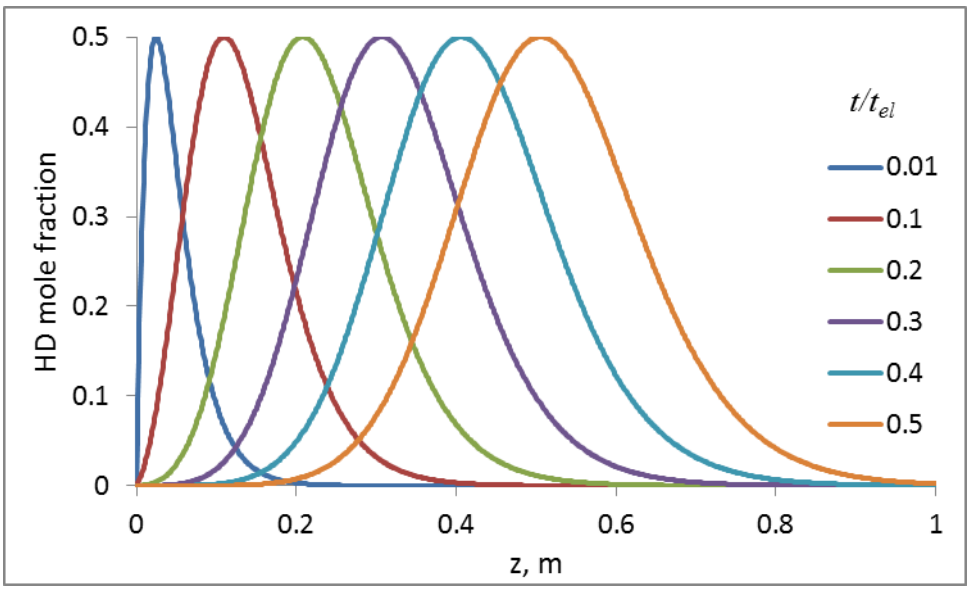

Figure 13. HD mole fractions versus position within tube at various times, expressed as a fraction of the elution time for k' = 100, L/v_0 = 1 s, α = 1.25, $v_k S/A_g$ = 31 s^{-1}.

The rate of the chemical reaction has different effects on the HD curve shape depending on the value of α. Figure 14 illustrates that the peak width grows as the -1/2 power of the rate constant when $\alpha = 1$, as expected from Clifford's result. When $\alpha > 1$, the peak width is inversely proportional to the rate constant.

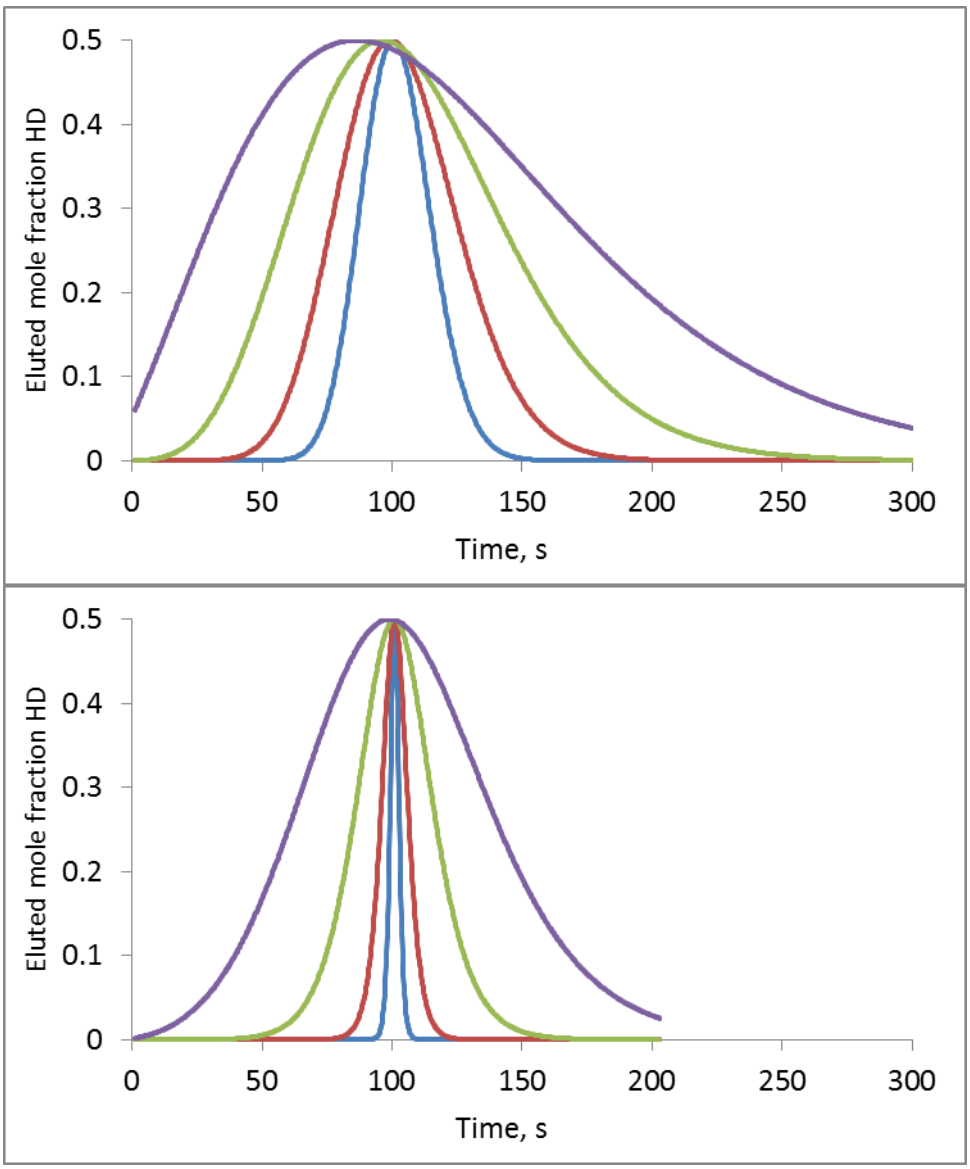

Figure 14. Eluted HD mole fractions versus time as predicted by Thomas for (top) $\alpha = 1$, (bottom) $\alpha = 2$. For both, $k' = 100$, $L/v_0 = 1$ s, $v_k S/A_g = 93$ s^{-1} for the sharpest curve, decreasing by factors of 3.

4.3. Numerical models of mass transport

In the 1940s and 50s, Thomas, Walter, Golay and others used profound mathematical methods to identify a subset of chromatography problems that can be described in detail. Currently, it is possible to substitute brains with brawn through the use of computational tools that numerically solve all varieties of the differential equations. Results presented here are obtained from the COMSOL finite element solver for both the one-dimensional case, and the two-dimensional case that includes radial diffusion. Because COMSOL is complicated and contains features that are not documented in detail, some of its solutions for the one-dimensional case were checked

against a simple finite-difference method implemented in C. The modeling results provide a clearer impression of peak shapes under the conditions described here. It is still desirable to have analytical expressions that capture the dependence of the results on experimental parameters. The models can be used to validate simple approximations of these. All of the cases described include a term for axial diffusion, because this term makes it easier for the solver to get through the very steep concentration gradient imposed by the initial conditions.

4.3.1. One-dimensional flow plus equilibrium reaction plus axial diffusion

If the chemical reaction is fast, an axial diffusion term can simply be added to the flow-plus-equilibrium reaction case considered in a previous section. This gives

$$\left[1+\frac{\alpha k'}{\left(1+(\alpha-1)(H/C_g)\right)^2}\right]\frac{\partial H}{\partial t}=D\frac{\partial^2 H}{\partial z^2}-v_0\frac{\partial H}{\partial z} \tag{70}$$

Implementation of this equation with the usual boundary conditions yields the results shown in Figure 15, where the gas velocity is varied, which affects the timescale of the simulated experiment; slower velocities allow more time for axial diffusion of gases. As with the rate constant dependence, the effect of diffusion is relatively small compared to the inherent broadening when $\alpha < 1$. There is an apparent dependence of peak width on gas velocity to the $-1/2$ power for $\alpha = 1$, and -1 power for $\alpha > 1$, at least for higher gas velocities. The peak shape becomes more skewed than in the kinetic case, as diffusive transport gets to be comparable to advective transport (flow), and the maximum value of the peak leads the elution time determined by gas velocity alone. The velocity scaling rules apparently lose their validity once the peak is highly skewed. When the gas velocity is zero, gas transport and reaction can still be driven by diffusion on a timescale similar to $(1+k')L^2/D$. This case is not easily captured by this numerical model because the outlet boundary condition requires a nonzero velocity, but it can be approached. Golay and Clifford restricted their analysis to the case where the width of the *H* front (or HD peak) are narrow compared to their position in the tube, but the numerical approach provides more detailed information about a wider range of conditions. While the oscillations observed for high values of α and v_0 in Figure 15 could have been corrected through more careful configuration of the solver, their existence illustrates the fact that cases involving reaction equilibrium (infinitely fast kinetics) can be more difficult to compute than cases of finite kinetics, as are presented in later sections.

As Figure 16 illustrates, the peak width scales as $(\alpha-1)^{-1}$ when $\alpha > 1$ and the peak width is much smaller than the elution time. This scaling is similar to that for the kinetically limited case described earlier. Axial diffusion is competing against the thermodynamic effect that sharpens the peak, so a strong α dependence can be expected.

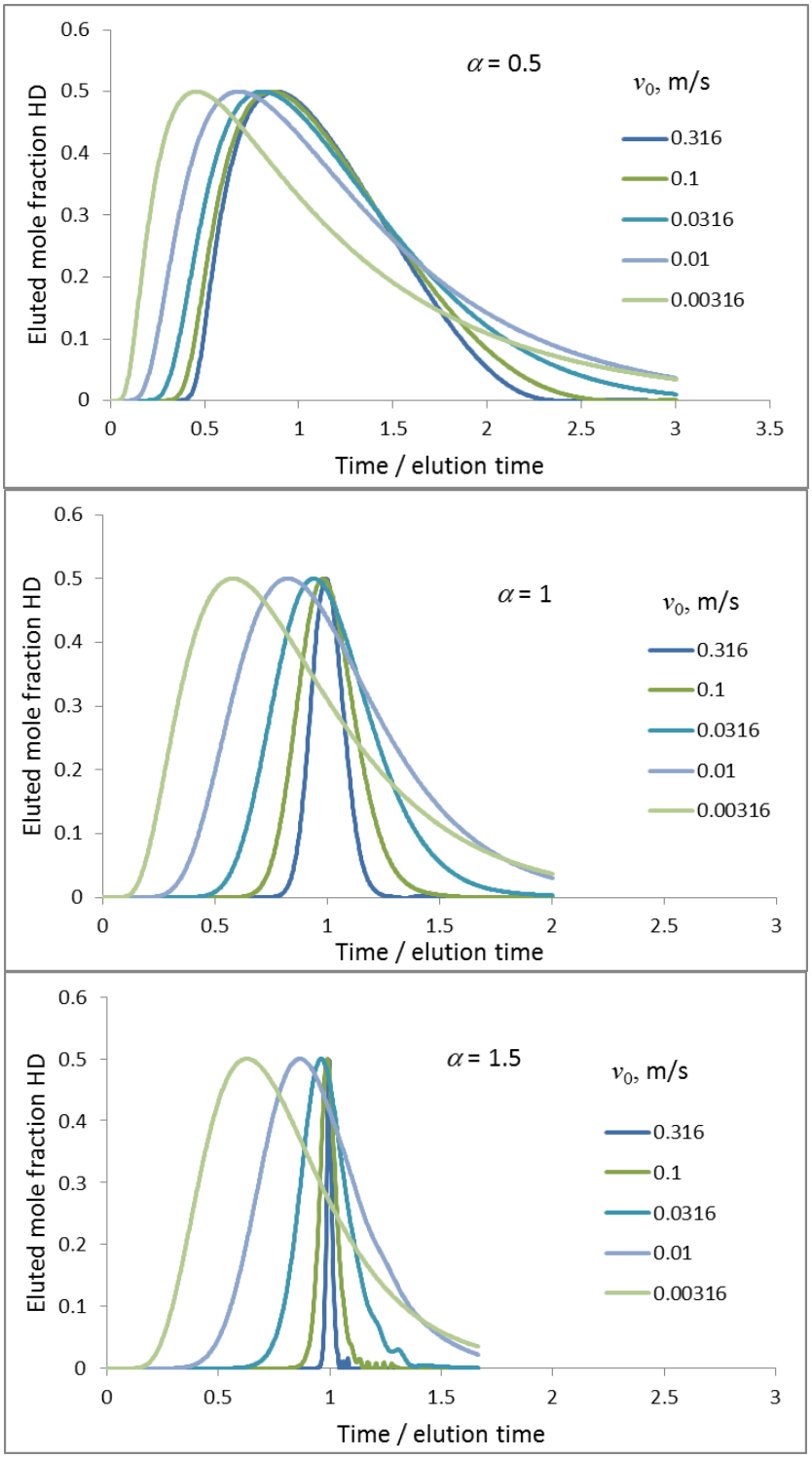

Figure 15. Eluted HD mole fractions versus time as predicted by COMSOL with chemical equilibrium for (top) $\alpha = 0.5$, (middle) $\alpha = 1$, (bottom) $\alpha = 1.5$. For each, $k' = 854$, $L = 0.1$ m, $D = 10^{-4}$ m^2/s, $v_0 = 0.316$ m/s for the sharpest curve, decreasing by factors of 3.16. Oscillations in the bottom curve are from a slightly misconfigured solver.

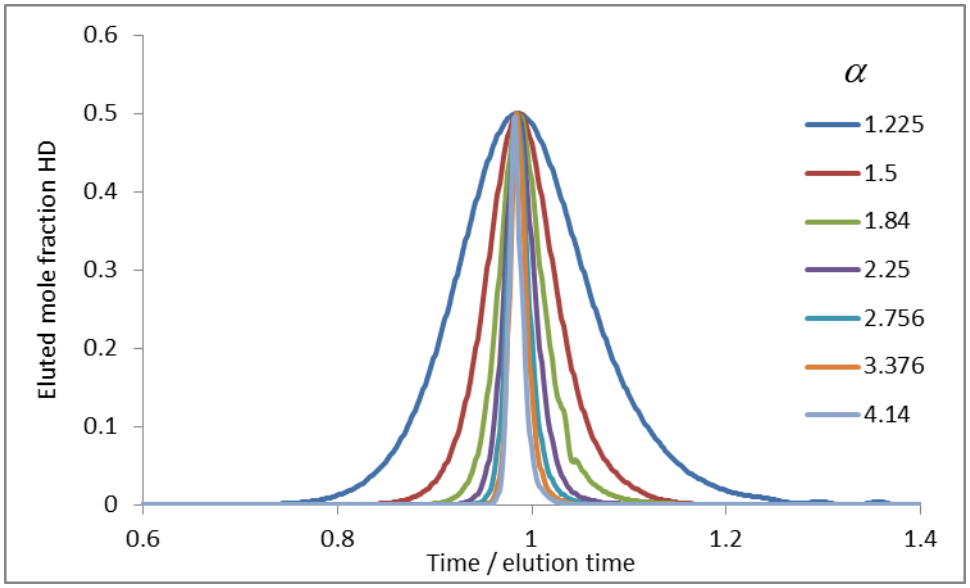

Figure 16. Eluted HD mole fractions versus time as predicted by COMSOL with fast kinetics. For each, k' = 854, L = 0.1 m, D = 10^{-4} m^2/s, v_0 = 0.1 m/s.

4.2.2. Flow plus reaction plus axial and radial diffusion

To incorporate radial diffusion, the same differential equation in the Golay section is used (or the version with radially independent gas velocity), along with a boundary condition modified to incorporate the nonlinear isotherm.

$$-D\frac{\partial H}{\partial r} = \frac{\alpha k' r_0}{2\left(1+(\alpha-1)(H/C_g)\right)^2}\frac{\partial H}{\partial t} \tag{71}$$

The effect of radial diffusion is illustrated in Figure 17 for both Poiseiulle flow (parabolic radial dependence of gas velocity) and plug flow (no radial dependence of gas velocity). Poiseiulle flow results in larger peaks, with a simple relationship: the plug-flow peaks are narrower by a factor of 0.75. The peaks are asymmetric, with a sharper tail on the leading side, whereas a peak limited by axial diffusion is sharper on the trailing side. The peak widths show a dependence weaker than $(\alpha-1)^{-1}$. In this case, the diffusion process is in series with the chemical reaction – that is, the gas must diffuse radially before it can react. For that reason, it makes sense that it would reduce the dependence of the peak width on chemical reaction effects, and reduce the ability of the reaction effects to sharpen the peak. Figure 17 shows that both flow types result in radial concentration variations, but confirms that the overall broadening is greater in the Poiseiulle case.

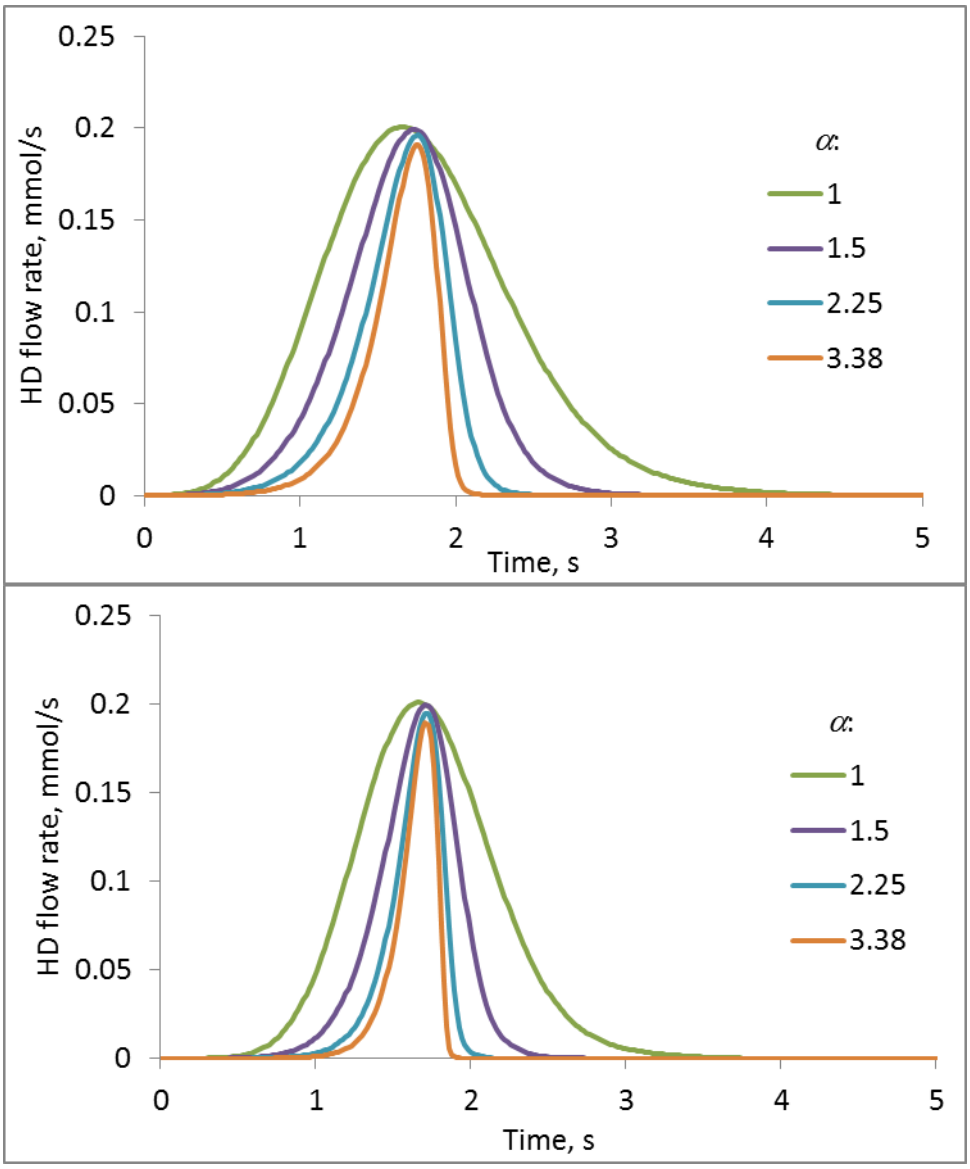

Figure 17. Eluted HD mole fractions versus time as predicted by COMSOL with fast kinetics for (top) Poiseiulle flow, (bottom) plug flow. For each, k' = 854, L = 0.1 m, D = 10^{-4} m^2/s, v_0 = 50 m/s, r_0 = $5x10^{-4}$ m.

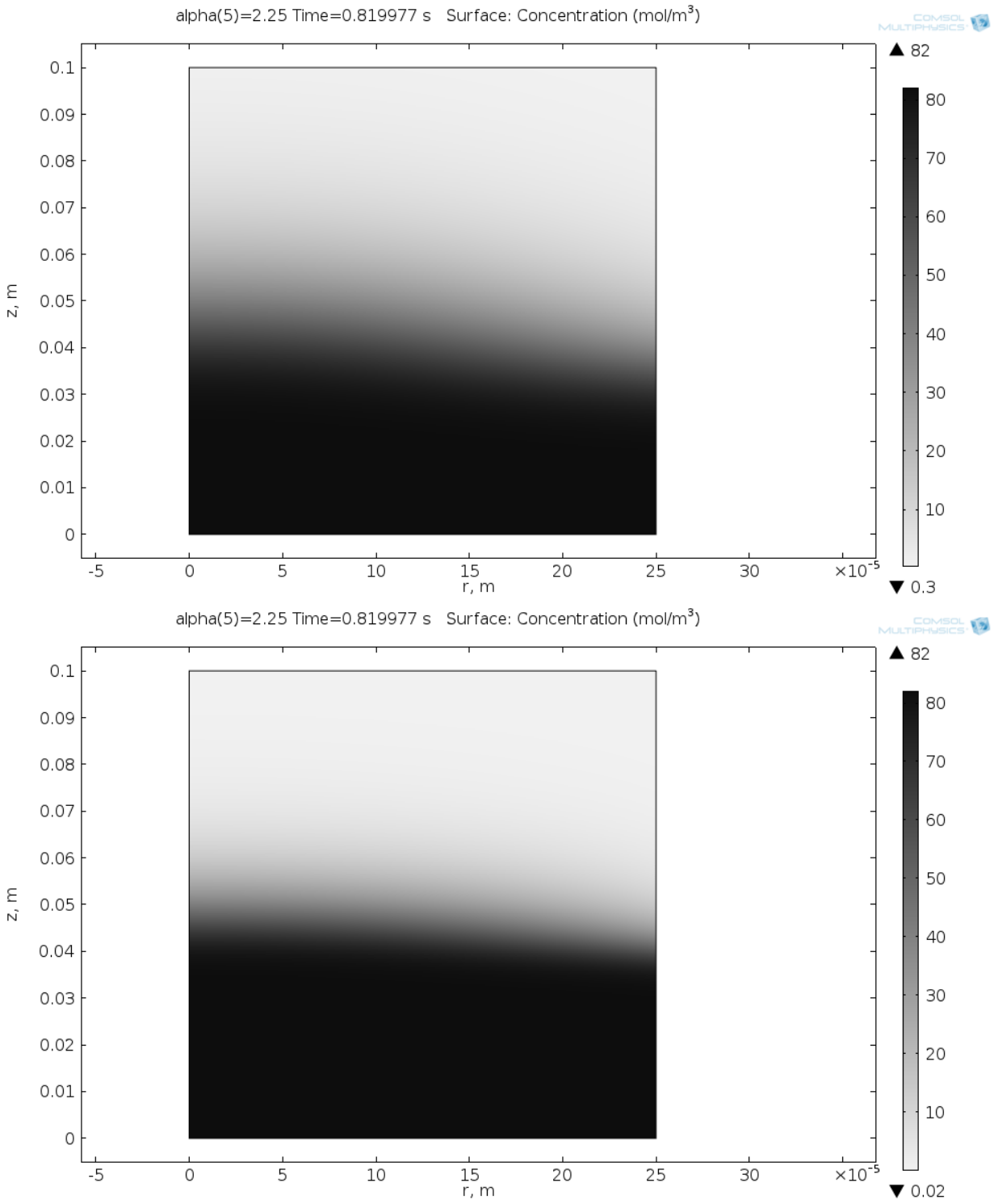

Figure 18. H concentration versus position at 0.2 s as predicted by COMSOL with fast kinetics for (top) Poiseiulle flow, (bottom) plug flow. For each, α = 2.25, k' = 854, L = 0.1 m, D = 10^{-4} m^2/s, v_0 = 50 m/s, r_0 = 5x10^{-4} m.

4.2.1. Flow plus reaction plus diffusion with slow kinetics

Numerical methods can also be used to study the combination of the mass transport effects with a slow chemical reaction. In this case, H_s must be recorded as a separate variable. The full rate law for H_s from Chapter 2 is combined with the mass balance and boundary conditions. Results from these combined models will be introduced in subsequent sections.

4.3. Analytical approximations to include mass transport

Hiester and Vermeulen have extended the solution obtained by Thomas to incorporate mass transport limits typical of ion exchange chromatography.[25] It has not been extended to incorporate axial or radial gas-phase diffusion, but it is still possible to compare these effects to kinetic and thermodynamic effects.

For $\alpha > 1$, if a broadening mechanism is present, such as axial diffusion, a finite amount of broadening will occur that is a balance between the broadening and sharpening mechanisms. The balance is a steady-state condition that can be assumed to apply at long times in long tubes, where the peak width would diverge for lower α values.

The *j* parameters can be generalized to

$$j_2 = (z/\sigma) \tag{72}$$

$$j_1 = \frac{1}{k'\sigma}(v_0 t - z) \tag{73}$$

allowing a more general σ that combines the various broadening effects. This follows the general strategy of Vermeulen. A numerical model that incorporates axial and radial diffusion along with second-order kinetics was implemented in Comsol. Comparison of the generalized Thomas solution to solutions computed in Comsol gives, at least in the range of $1 < \alpha < 5$,

$$\sigma = \left(\frac{1.25D}{v_0} + \frac{v_0 r_0}{2v_k} + \frac{(1+\alpha)v_0 r_0^2}{8D} \right) \tag{74}$$

The second and third term could be thought of as v_0 times the sum of series resistances including a kinetic term $1/(v_k S/A_g)$ and 1/rate of radial diffusion = $4D/r_0^2$. If there is no radial dependence of gas velocity, a good fit to Comsol simulations is obtained if the third term be multiplied by 0.75. A generalized version of the solution for $\alpha > 1$ incorporating these broadening terms is

$$\frac{H}{C_g} = \frac{1}{1+\exp\left[\frac{(\alpha-1)(1+k')}{k'\sigma} \left(z - \frac{v_0}{(1+k')} t \right) \right]} \tag{75}$$

For α > 1.5, Comsol results are reasonably well described by the following expression for the width of the HD peak (defined by its area divided by its peak value):

$$\frac{\sigma_{\mathrm{HD}}}{L} = \frac{4}{\alpha - 1}\left(\frac{1.25D}{v_0 L} + \frac{v_0 r_0}{2v_k L} + \frac{(\alpha+1)v_0 r_0^2}{8DL}\right) \tag{76}$$

The degree of accuracy of this generalized solution is illustrated in Figure 19 by comparison to COMSOL models. The kinetically limited case is essentially an exact match, as expected. The diffusive cases have different peak shapes. The approximate solution is far from perfect, but much better than would be obtained by neglecting the mass transport processes. It is suitable as an initial estimate that can be confirmed by a numerical solution of the equations.

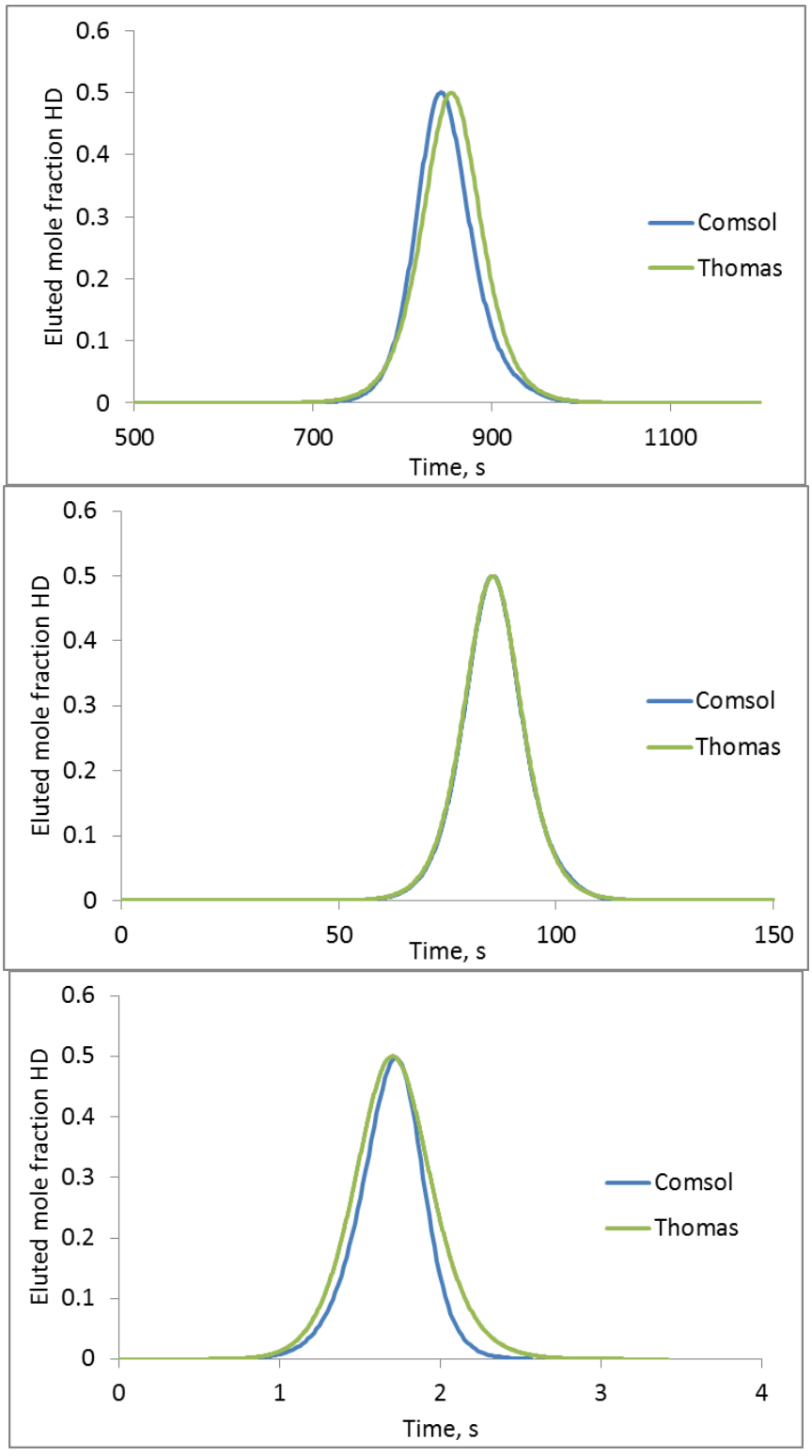

Figure 19. Eluted HD mole fractions versus time as predicted by COMSOL and the generalized Thomas equation for (top, axial diffusion-limited) D = 10^{-4} m^2/s, v_0 = 0.1 m/s, v_k = 1 m/s; (middle, kinetically limited) D = 10^{-5} m^2/s, v_0 = 1 m/s, v_k = 10^{-2} m/s; (bottom, radial diffusion-limited) D = 10^{-5} m^2/s, v_0 = 50 m/s, v_k = 1 m/s. For each, α = 1.5, k' = 854, L = 0.1 m.

4.4. Performance optimization

The previous section provided an expression for σ/L that resembles the theoretical plate expression derived by Clifford. These differ in their coefficients, and the fact that σ/L is squared in the case of a first-order reaction, but not in the case of the second-order reaction. Squaring σ/L in the definition of the number of plates makes sense in linear chromatography, because the peak broadens in proportion to $L^{1/2}$, but the peak does not broaden for a second-order reaction when $\alpha > 1$. The lack of broadening changes the tradeoff between number of plates and the rate of their creation, because plates are created in direct proportion to both time and length, and their rate of creation is constant. The tradeoff is instead drawn from the pressure drop constraint, which constrains r for a given L. In that case, L can be chosen, and then the optimum v_0 determined. The number of plates and elution time can be determined from these, and L adjusted as necessary. An expression to be optimized that is similar to the case of the first-order reaction is

$$\frac{1}{N} \propto \frac{\sigma_{\mathrm{HD}}}{L} = \frac{4}{\alpha - 1}\frac{v_0}{L}\left(\frac{1.25D}{v_0^2} + \frac{1}{v_k}\left(\frac{40\mu v_0 L}{C_g R_g T}\right)^{1/2} + \frac{(\alpha+1)}{D}\frac{20\mu v_0 L}{C_g R_g T}\right) \tag{77}$$

For this problem, the number of plates is defined without squaring σ/L. Plots of N and Nv_0/L as a function of v_0 and L can aid in the optimization as before, and they are very similar in form.

4.5. Optimization with sharpening

An opportunity for further optimization of the plate production rate (or plate duration) exists for the case of second-order kinetics, but it is not easily addressed by the Thomas equation or the theoretical plate treatments described above. The Thomas equation describes the response to a step input, and the plate treatment considers the steady-state condition where the peak width is constant. Figure 13 shows the transition from a step function to a peak of finite, constant width, as predicted by the Thomas function. As can be shown by numerical modeling, this process also occurs for the opposite case: if the initial condition is a broad smear of H and H_s across the length of the column, the column still makes a transition to the same peak of finite, constant width. This is illustrated in Figure 20, where the initial concentrations are high over the first third of the column. The H front achieves its steady-state sharpness by the time it is halfway through the column.

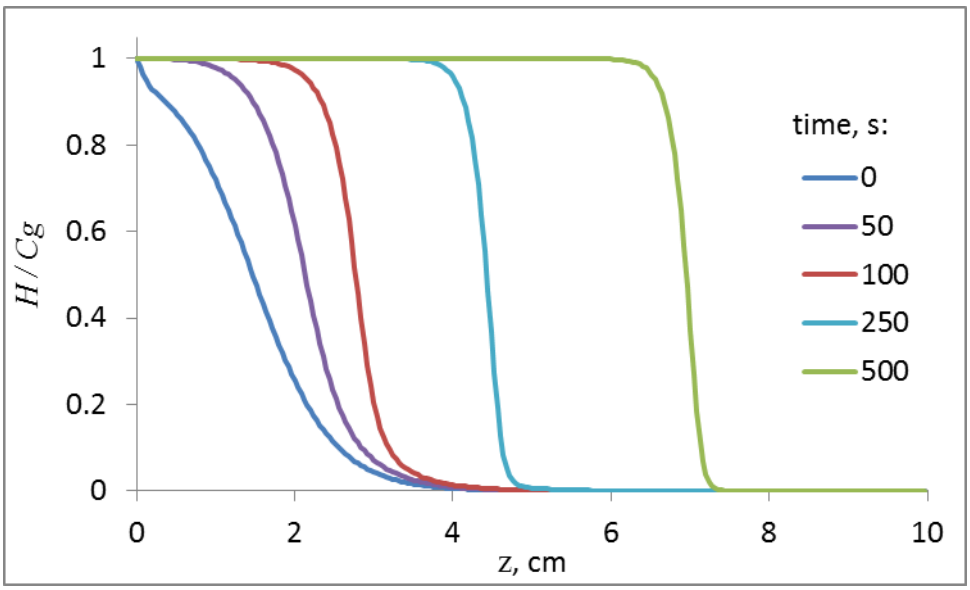

Figure 20. H concentrations inside a column that started with a broad axial distribution of H and H_s. D = 10^{-4} m^2/s, v_0 = 10 cm/s, v_k = 2.75 cm/s,ID 0.01 cm, α = 3.0, k' = 854, L = 10 cm.

This self-correcting behavior could be exploited to improve the plate production rate by operating the column at a gas velocity that is significantly faster than the optimum predicted by the previous section, causing a broad axial distribution of H_s, but not enough to cause a significant elution of H. Then the velocity could be reduced to the optimum, sharpening the distribution to the same shape it would be if the experiment had been performed more slowly, and allowing a sharp elution in a shorter period of time. Design of the optimal time-dependent velocity profile is beyond the scope of this report, but this topic is introduced to clarify that performance improvements may be obtainable if a designer goes beyond simply operating at a constant velocity.

5. HIERARCHICAL POROSITY

5.1. Solid-phase diffusion

The previous chapters focus on the connection between gas transport and reaction kinetics, ignoring transport in the solid phase. However, in the examples described, the fraction of the tube's cross-sectional area occupied by the solid phase is comparable to that of the gas phase. There is no flow mechanism in this phase, so diffusion is the only means of transport. Chapter 2 noted that the diffusion constant in the solid is 20,000,000 times lower than in the gas phase. In the same amount of time, hydrogen can diffuse about 4,000 times farther in the gas phase. Another important aspect of this is that the concentration in the solid phase is about 1000 times higher, so to obtain a given flux, the relative concentration gradient in the solid must be about 20,000 times that in the gas. The following equations describe this case:

$$\frac{\partial H}{\partial t} = D\frac{\partial^2 H}{\partial z^2} + D\frac{1}{r}\frac{\partial}{\partial r}\left(r\frac{\partial H}{\partial r}\right) - v_0\frac{\partial H}{\partial z} \tag{78}$$

$$\frac{\partial H_s}{\partial t} = D_s\frac{\partial^2 H_s}{\partial z^2} + D_s\frac{1}{r}\frac{\partial}{\partial r}\left(r\frac{\partial H_s}{\partial r}\right) \tag{79}$$

and at the phase boundary,

$$R = -D\frac{\partial H}{\partial r} = -D_s\frac{\partial H_s}{\partial r} = \alpha k\frac{H}{C_g}\left(1-\frac{H_s}{C_s}\right) - k\frac{H_s}{C_s}\left(1-\frac{H}{C_g}\right) \tag{80}$$

The usual inlet, outlet, and initial conditions apply, and all other boundaries of the solid phase have zero normal slope.

Figure 21 shows two examples of COMSOL predictions of this case. Solid-phase diffusion limits transport significantly more than gas-phase radial diffusion at high gas velocities. Previous chapters (that neglect solid-phase diffusion) have shown that the optimum velocity for this geometry is around 1 m/s. Under these conditions, that value is a lower; Figure 21 shows that the phases are not far from equilibrium at about 0.1 m/s. It is reassuring that, despite the very small diffusion constant for the solid phase, transport from the solid phase can still proceed at a respectable rate in this geometry. Near equilibrium, the front in the solid phase runs slightly ahead of that in the gas phase due to the nonlinear shape of the isotherm.

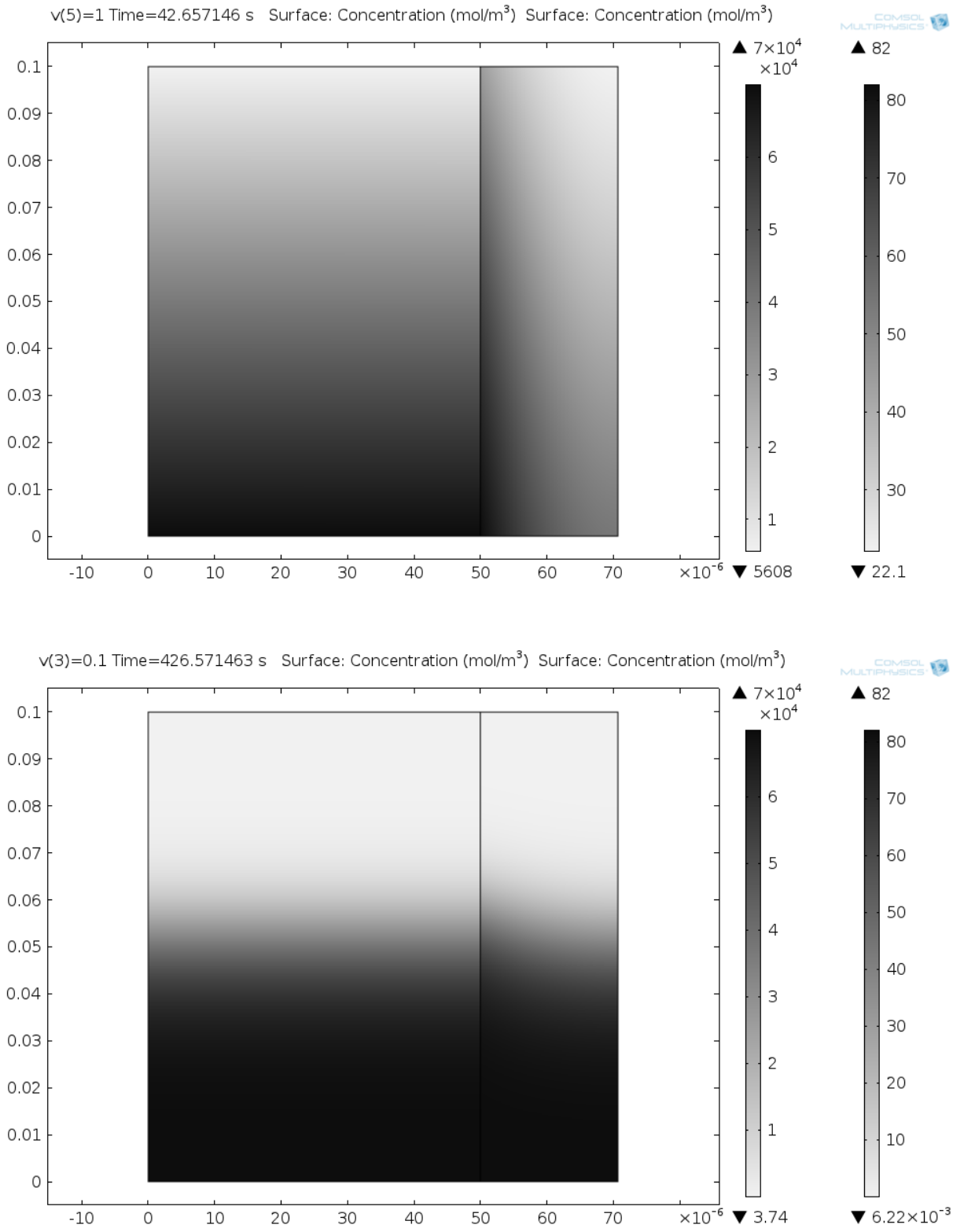

Figure 21. Maps of H (left region) and H_s (right region) in mol/m^3 versus position in the column (m) as predicted by COMSOL for gas velocities of (top) 1 m/s and (bottom) 0.1 m/s for D = 10^{-4} m^2/s, v_k = 0.55 m/s, D_s = 5x10^{-12} m^2/s, α = 2, k' = 853, r_0 = 100 µm.

Similar COMSOL calculations were made using an anisotropic diffusion constant to omit the effect of solid-phase axial diffusion. Any differences present were quite small.

Golay has provided a plate expression for solid-phase diffusion in a tubular gas chromatography column. It captures the concepts described above, and provides a quantitative analytical estimate of this effect in comparison to other mechanisms that limit peak sharpness.

$$\frac{1}{N} = \frac{C_g v_0 \left(OD^2 - ID^2\right)}{24 C_s D_s L} \tag{81}$$

This predicts about 1 plate for the top plot of Figure 21, and about 10 for the bottom plot, which is approximately consistent with the ratio of front width to column length observed there.

5.2. Linear driving force approximation

A simplified treatment of solid-phase diffusion can be obtained using a generalization of Glueckauf's linear driving force approximation.[26] This reduces the dimensionality of H_s that must be accounted for, by relating the surface concentration to the average bulk concentration $\overline{H}_s$, both of which are independent of radius. If axial diffusion can be considered negligible, then H_s and $\overline{H}_s$ can follow ordinary differential equations. The simplification works for a set of simple geometries such as a sphere, cylinder, or a hollow tube, at timescales exceeding an appreciable fraction of the square of a characteristic length of the geometry (such as radius) divided by the diffusion constant. That is, the approximation does not apply at very short times after an abrupt change when the concentration gradient near the phase boundary is very large. When applying the hollow tube model to this problem, axial diffusion in the solid must be negligible. As implemented here, H_s is reinterpreted as the solid-phase hydrogen concentration near the surface.

$$\frac{\partial \overline{H}_s}{\partial t} = \frac{24}{(5\xi + 3)(\xi - 1)^2} \frac{D_s}{r_0^2} \left(H_s - \overline{H}_s\right) \tag{82}$$

Here, $\xi = OD/ID$. To incorporate this into a 1D model that includes axial diffusion and flow in the gas phase, along with finite reaction kinetics,

$$\frac{\partial H}{\partial t} = D \frac{\partial^2 H}{\partial z^2} - v_0 \frac{\partial H}{\partial z} - \frac{Sk}{A_g} \left[\alpha \frac{H}{C_g} \left(1 - \frac{H_s}{C_s}\right) - \frac{H_s}{C_s} \left(1 - \frac{H}{C_g}\right) \right] \tag{83}$$

$$\frac{\partial H_s}{\partial t} = \frac{Sk}{S\delta} \left[\alpha \frac{H}{C_g} \left(1 - \frac{H_s}{C_s}\right) - \frac{H_s}{C_s} \left(1 - \frac{H}{C_g}\right) \right] - \left(\frac{A_s}{S\delta} - 1\right) \frac{\partial \overline{H}_s}{\partial t} \tag{84}$$

where δ is a nominal thickness of the surface layer, perhaps one percent of *OD*. The result is not expected to be sensitive to small changes in this parameter. If so, the assumptions for the given situation should be examined. For fast kinetics, the surface layer can be accounted for more simply:

$$\frac{\partial H}{\partial t} = D\frac{\partial^2 H}{\partial z^2} - v_0\frac{\partial H}{\partial z} - \frac{A_s}{A_g}\frac{\partial \overline{H}_s}{\partial t} \tag{85}$$

$$\frac{\partial \overline{H}_s}{\partial t} = \frac{24}{(5\xi+3)(\xi-1)^2}\frac{D_s}{r_0^2}\left(\frac{\alpha C_s H}{C_g + (\alpha-1)H} - \overline{H}_s\right) \tag{86}$$

However, COMSOL can often converge more quickly for cases of finite kinetics.

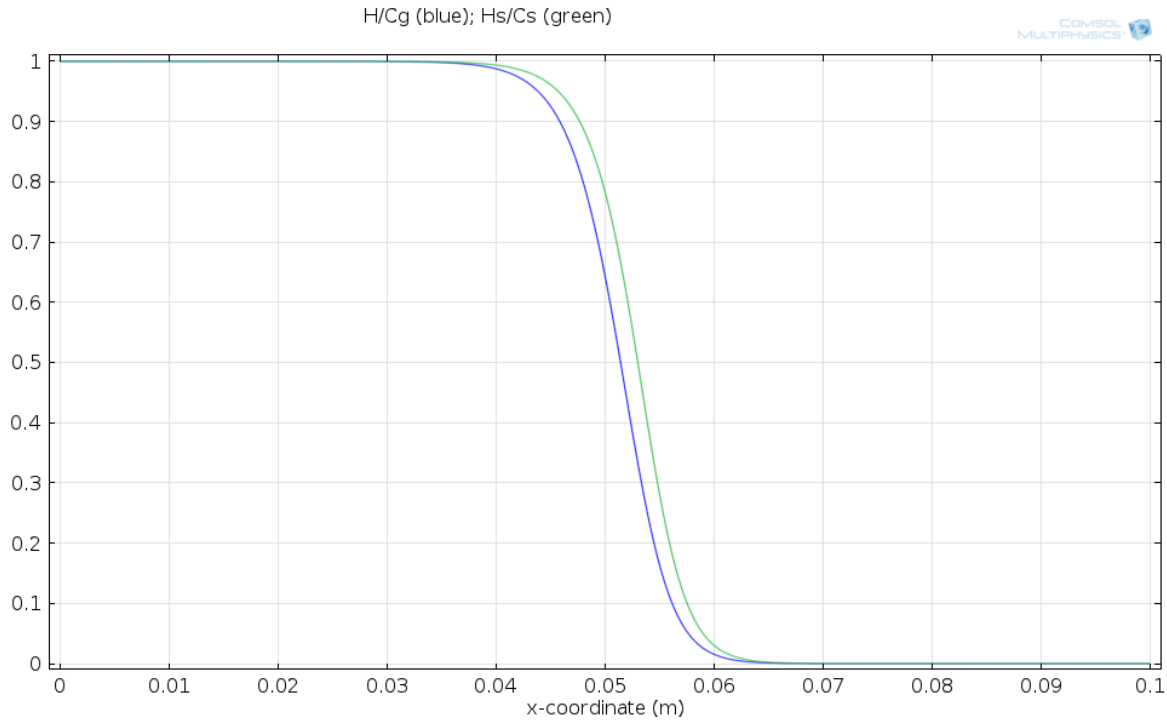

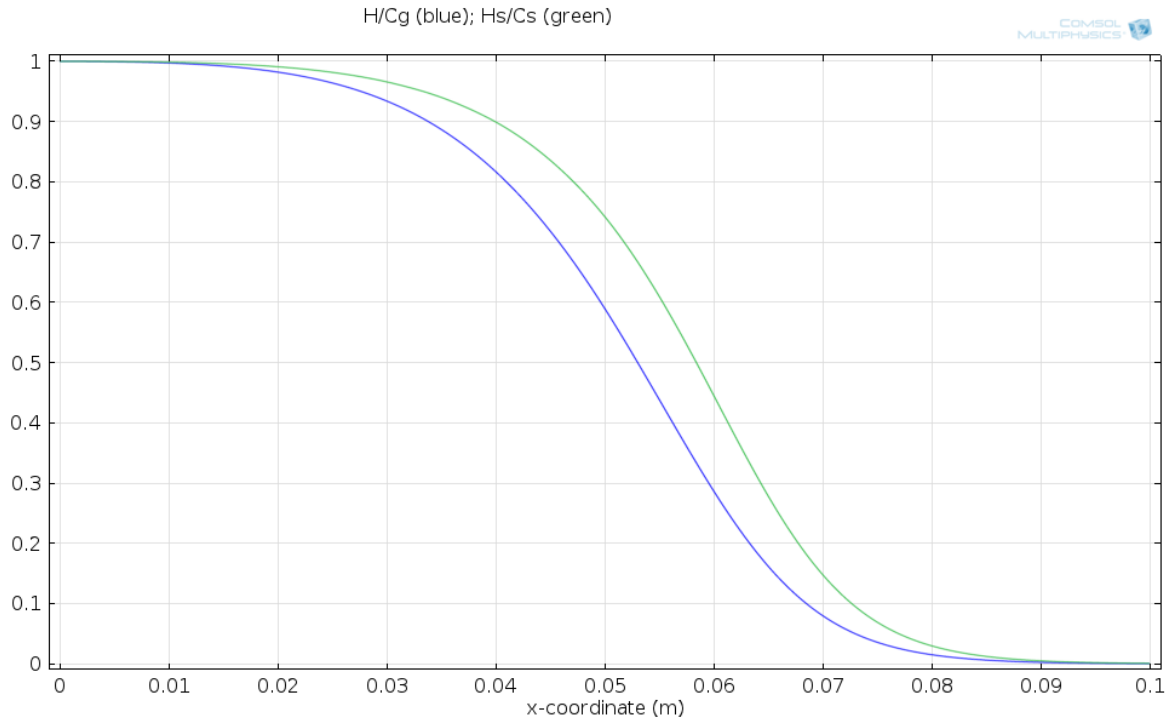

Figure 22. Plots of H (blue) and H_s (green) in mol/m^3 versus position in the column (m) as predicted by COMSOL with a linear driving force approximation for solid-phase diffusion, using gas velocities of (top) 0.01 m/s and (bottom) 0.1 m/s, and D = 10^{-4} m^2/s, D_s = 5x10^{-12} m^2/s, α = 2, k' = 853, r_0 = 100 μm.

Figure 22 illustrates that a 1D model treating solid-phase diffusion with the linear driving force approximation gives results similar to that of the full 2D axisymmetric model, where the front in the solid phase leads that in the gas phase at low velocities, and at higher velocities, the front is significantly broadened in each phase, and there is a greater difference between the phases.

When generalizing the Thomas solution, Vermeulen also suggests a solid diffusion term in the theoretical plate formula based on Glueckauf's linear driving force model. It takes the form v_0/L divided by the coefficient in the linear driving force equation. The concentration ratio between the phases would presumably be retained, leading to

$$\frac{1}{N} = \frac{(5\xi + 3)(\xi - 1)^2 C_g v_0 r_0^2}{24 C_s D_s L} \tag{87}$$

This expression is quite similar to the expression derived by Golay, who did not make thorough considerations of the annular geometry of the solid phase, effectively using $\xi^2 - 1$ as the function of ξ. The Glueckauf version increases more steeply, reflecting that the volume increases more than linearly with *OD*, so it is likely a better model of thick solid layers.

5.3. Concept of hierarchical porosity

A useful strategy to reduce any mass transport limitations caused by long-distance diffusion in the solid phase, and also to increase surface area to improve the molar throughput of the chemical reaction, is to include pores in the solid phase. An example geometry is an array of cylindrical pores of diameter much smaller *ID* that extend radially from the gas-solid boundary to the outer diameter, packed so that the pore volume fraction equals the solid volume fraction (a 50% porous solid phase). Hydrogen can diffuse through the gas phase more quickly than through the solid phase, and the pore surface area is much higher than that of the macroscopic gas-solid boundary. This scenario is easily modeled in COMSOL by combining several concepts introduced in this report. More elaborate arrangements could be envisioned in which flow occurs in the pore channels, but that will not be considered here. Porous solid phases are widely used in analytical (first-order) gas chromatography, even though the solid phase is usually thinner than described here. In that context, this geometry is known as "porous-layer open tube" (PLOT).

5.4. Purely diffusive channel

To understand the hierarchical arrangement, it is helpful to first understand the behavior of an individual pore in the solid phase, where there is no flow, and the pore has only one entrance. Hydrogen transport in a diffusion channel could be described by

$$\frac{\partial H}{\partial t} = D\frac{\partial^2 H}{\partial z^2} - \frac{A_s}{A_g}\frac{\partial H_s}{\partial t} \tag{88}$$

where H is fixed at the inlet and there is a zero-slope boundary condition at the end.

Incorporating first-order reaction equilibrium leads to

$$\frac{\partial H}{\partial t} = \frac{D}{1+\alpha k'}\frac{\partial^2 H}{\partial z^2} \tag{89}$$

This is basically the diffusion equation with a reduced diffusion constant. H_s obeys the same differential equation, and differs from H only by the scaling factor

$$H_s = \alpha k' H \tag{90}$$

For the second-order reaction, it is

$$\left[1+\frac{\alpha k'}{\left(1+(\alpha-1)\left(H/C_g\right)\right)^2}\right]\frac{\partial H}{\partial t} = D\frac{\partial^2 H}{\partial z^2} \tag{91}$$

which is more complicated, but is easily modeled in Comsol. Figure 23 shows the molar flow rate from a diffusive channel after a concentration step at the inlet. Higher values of α result only in small changes in flow rate, mostly at longer times. Figure 24 shows the HD concentration within the channel at various times. An HD peak is present at short times, but it is quite broad, and only slightly sharpened by increased α. It soon transforms into a monotonic gradient along the channel length, and decreases to zero as the reaction completes.

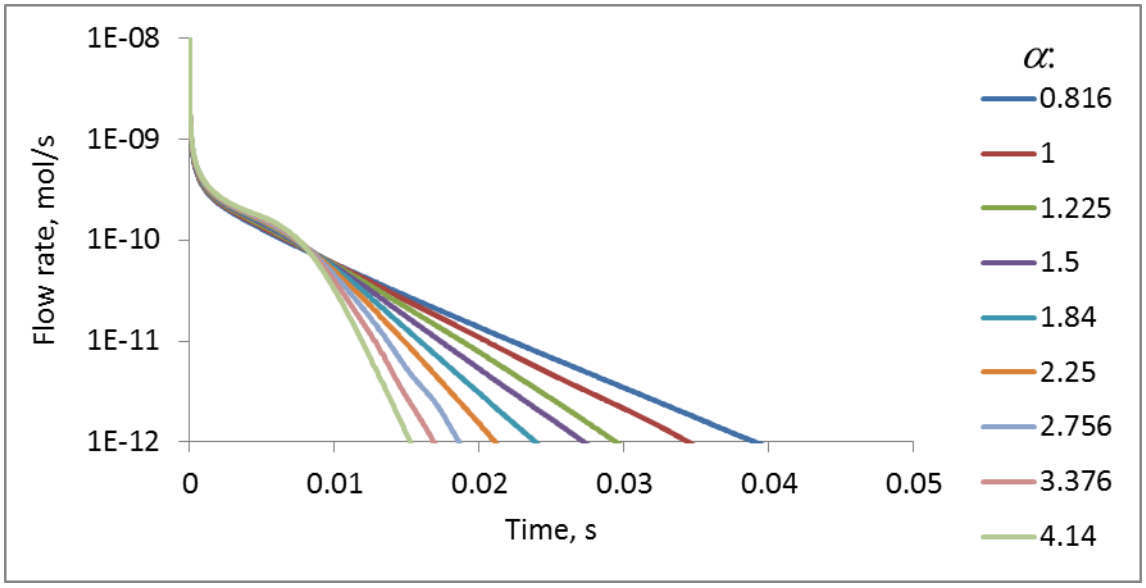

Figure 23. Molar flow rate from diffusive channel when the inlet H is stepped from zero to C_g with ID 1 μm, OD 1.41 μm, D 1 cm^2/s, and L 41.4 μm.

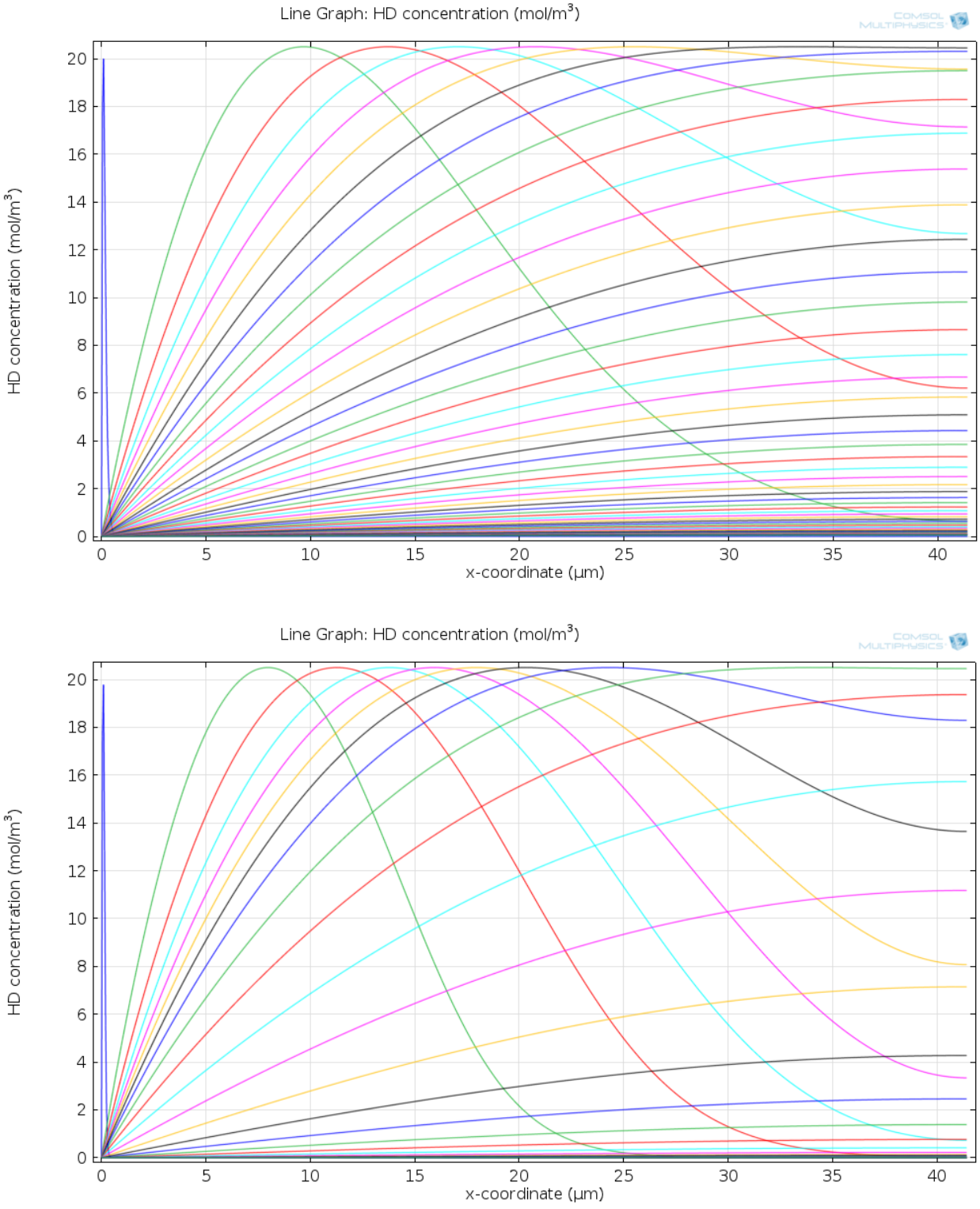

Figure 24. HD concentration in single-ended diffusion channel at various times when (top) a = 1, (bottom) a = 4.14. At increasing times, the peaks move from left to right. After the peaks have flattened, the curves move down with time. Colors match at equal times for the two plots.

5.5. Porous stationary phase

A one-dimensional model of transport in a pore is a convenient simplification, but the problem is still complicated when there is a very large number of such pores, and the state of each depends on their axial position. This problem has been addressed by Newman *et al*. for the case of porous battery electrodes,[27] as well as by common treatments of packed-powder columns. Both H and H_s are treated as continuous functions throughout the porous solid, regardless of whether a given microscopic point is within the solid volume or pore volume. However, the concentrations in the porous region are those in their respective phases: moles per pore volume, or moles per solid volume. The porosity ϕ is the ratio of pore volume to total volume, and can be used to convert between pore, solid, and total volumes. The term "stationary phase" is a generalization of what previous sections have called the solid phase. It is a region consisting of the solid along with gas that is not flowing. The region where the gas is flowing is the mobile phase.

For a 2D axisymmetric model of a tube with a porous stationary phase, the mobile phase can be described as in section 3.1.4. To describe H in the stationary phase, an equation analogous to that in section 5.4 can be used, noting that the pores are now taken to extend radially rather than axially.

$$\frac{\partial H}{\partial t} = \frac{D}{r}\frac{\partial}{\partial r}\left(r\frac{\partial H}{\partial r}\right) - \frac{A_s^*}{A_g^*}\frac{\partial H_s}{\partial t} \tag{92}$$

Here, the asterisks are meant to indicate pore geometry rather than tube geometry. That area ratio is

$$\frac{A_s^*}{A_g^*} = \frac{1-\phi}{\phi} \tag{93}$$

The assumption of straight, uniform radial pores and walls is not very realistic if the porous layer is thick, but the current treatment will ignore this. Especially if the pores have axial interconnections, an axial diffusion term can be included. Considerations of the effect of three-dimensional porosity on the diffusion constant can get complicated, but often do not significantly improve accuracy. Including the axial diffusion term may allow a simulation to proceed with larger timesteps without significantly changing the result, so it can be practical to include it. The results shown in this section include axial diffusion in the stationary phase for COMSOL calculations.

H can be considered continuous across the boundary between mobile and stationary phases. However, the concentrations have different interpretations in each region: moles per total volume in the mobile phase, and moles per pore volume in the stationary phase. This can be accounted for by a flux discontinuity at the boundary. The outward flux at the boundary just inside the mobile phase is $-D\partial H/\partial r$, whereas just inside the stationary phase it is $-D\partial(\phi H)/\partial r$, measuring flux in terms of moles per total boundary area per unit time. The net flux created at

the boundary must be equal to the difference of these: $-D(1-\phi)\partial H/\partial r$.[28] This assumes that $\partial H/\partial r$ is continuous across the boundary, which is true if there is rapid equilibration with the solid phase right at the boundary, and thus no flux into the solid. Essentially, this boundary condition destroys the flux resulting from the fictitious presence of *H* in the solid. This condition is necessary to obtain mass balance. Further complications, which are ignored here, can impose mass transport limitations, such as the entropic barrier at the pore entrance.[29]

The model geometry does not capture microscopic transport along the pore radius, but that is still of interest, because a key goal is to determine how big or small the pores must be. That effect can still be captured using the linear driving force model, which is only considered here for transport in the solid, and not for gas transport along the pore radius. $\overline{H}_s$ can be described as in Section 5.4, with the tube radius replaced by the pore radius r_p, and noting that, in the context of a pore, $\xi = \phi^{-1/2}$.

$$\frac{\partial \overline{H}_s}{\partial t} = \frac{24\phi^{3/2}}{\left(5+3\sqrt{\phi}\right)\left(1-\sqrt{\phi}\right)^2}\frac{D_s}{r_p^2}\left(H_s - \overline{H}_s\right) \tag{94}$$

Transport from *H* to $\overline{H}_s$ must be broken into two steps, with H_s as an intermediate.

$$\frac{\partial H}{\partial t} = \frac{D}{r}\frac{\partial}{\partial r}\left(r\frac{\partial H}{\partial r}\right) - \frac{S^* k}{A_g^*}\left[\alpha\frac{H}{C_g}\left(1-\frac{H_s}{C_s}\right) - \frac{H_s}{C_s}\left(1-\frac{H}{C_g}\right)\right] \tag{95}$$

$$\frac{\partial H_s}{\partial t} = \frac{S^* k}{S^*\delta}\left[\alpha\frac{H}{C_g}\left(1-\frac{H_s}{C_s}\right) - \frac{H_s}{C_s}\left(1-\frac{H}{C_g}\right)\right] - \left(\frac{A_s^*}{A_g^*}\frac{A_g^*}{S^*\delta} - 1\right)\frac{\partial \overline{H}_s}{\partial t} \tag{96}$$

$$\frac{A_g^*}{S^*} = \frac{r_p}{2} \tag{97}$$

The capacity of the stationary phase is such that

$$k' = \frac{\left((1-\phi)C_s + \phi C_g\right)A_s}{C_g A_g} \tag{98}$$

Figure 25 illustrates that the incorporation of 5 µm diameter pores into the stationary phase effectively cures the solid-phase mass transport limitation described for a nonporous solid phase as described in Section 5.1. This justifies the use of simpler models that neglect solid-phase transport, as used in the previous chapters. However, it is important to have this more complex model to verify that the stationary-phase porosity achieves its goal.

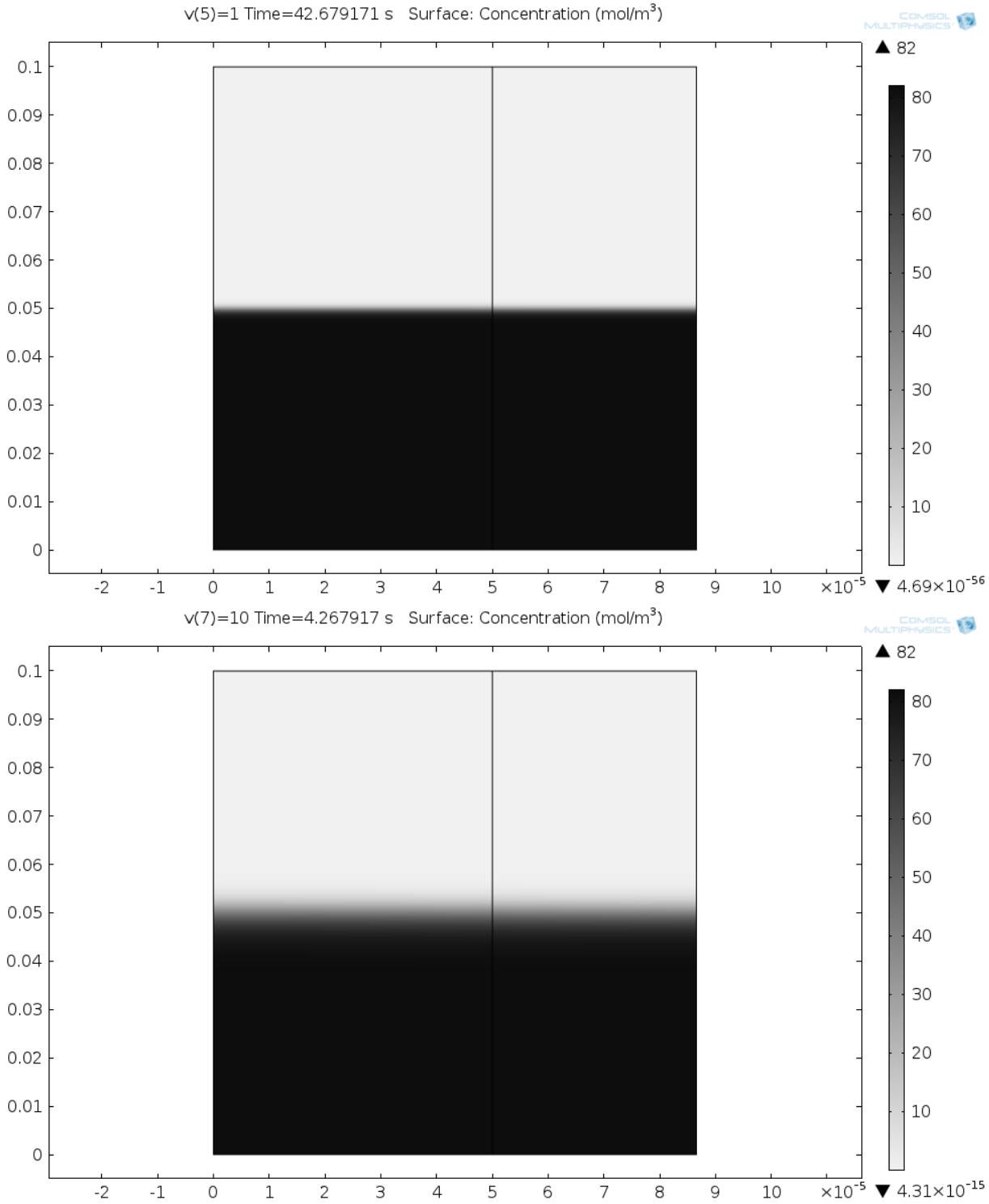

Figure 25. Maps of H in the mobile phase (left) and stationary phase (right) in mol/m^3 versus position in the column (m) as predicted by COMSOL for gas velocities of (top) 1 m/s and (bottom) 10 m/s for D = 10^{-4} m^2/s, v_k = 0.55 m/s, D_s = 5x10^{-12} m^2/s, α = 2, k' = 853, r_0 = 100 µm, r_p = 5 µm.

From these considerations, a more complete plate expression can be proposed:

$$\frac{1}{N} \propto \frac{\sigma_{\mathrm{HD}}}{L} = \frac{4}{\alpha - 1}\left(\frac{1.25D}{v_0 L} + \frac{v_0 r_p}{4(\xi - 1)\phi v_k L} + \frac{(\alpha + 1)\xi v_0 r_0^2}{8DL} + \frac{\left(1 - \sqrt{\phi}\right)^2 C_g v_0 r_p^2}{4\phi^{3/2} C_s D_s L} \right) \tag{99}$$

where ξ refers to the tube geometry, and not the pore geometry. The first term is the same axial diffusion term as in Section 4.3. The second term is the same kinetic term, but divided by the ratio of the surface area of a pore wall to the corresponding area of the boundary between the mobile and stationary phases. The third term is the same radial diffusion term, but multiplied by ξ to reflect that the gas must diffuse across both the flow channel radius and much of the pore length. Because the gas is absorbed along the length of the pore, this term is likely a more complicated function of ξ; a linear relationship is proposed as a simple estimate. The fourth term accounts for solid-phase diffusion, as discussed at the end of section 5.2, with the porosity substitution as described earlier in this section, and approximating $5 + 3\sqrt{\phi} \approx 6$. Some effort would be required to validate the dependence of each parameter through COMSOL modeling, but this plate expression may be a useful starting point for estimation of the performance of a hydride tube with a porous stationary phase.

6. IMPLEMENTATIONS

6.1. Studies of chemical reaction kinetics

An open-tube reactor that operates at well defined values of v_0 and r would be ideal for the study of the isotope exchange reaction. In this case, and at values of those parameters where diffusive transport does not contribute to HD peak width, v_k can be reliably extracted from that peak width. That measurement would apply to a given hydride material in a given form. Using an ample amount of hydride material increases k', slowing the elution process and allowing HD concentrations to be measured on a convenient timescale. However, the material form must be one that ensures that any solid-phase transport processes are fast, and the geometry well defined so the surface area is known.

6.2. Preparative scale

The total number of moles of hydrogen held in the tube, n, is

$$n = \left(C_g A_g + \phi C_g A_s + (1-\phi) C_s A_s\right) L = C_g A_g L (1 + k') \tag{100}$$

This number can be increased by making the tube longer or wider, but this changes its flow properties. Hypothetically, more moles can be held in a column if many tubes in are placed parallel. Prior studies caution against this, due to sensitivity to slight variations in tube diameter.[30] Distribution of eluent to the inlet of each tube, and collection of eluate from each outlet, will be increasingly challenging if a tube array becomes extremely thin and wide. One solution to the diameter variation is to occasionally shuffle flow between tubes, such as by stacking short segments of tube arrays. An inert material of similar geometry at the entrance and exit could help distribute flow. These are expected to be fruitful topics for future study.

6.3. Packed columns

For comparison of the open tube model to columns made of packed powder, only a few variable substitutions are needed. Two key parameters of the packed column are its cross-sectional area A_c and its porosity (void fraction) ϕ_c.

$$\phi_c = 1 - \frac{\rho}{\rho_{bulk}} \tag{101}$$

Where the densities ρ are of the packed column and of a nonporous slab of the hydride. Table 2 describes most of the necessary changes.

Table 2. Transformations between open-tube geometry and packed column geometry.

Open Tube	Packed Column
A_g	$\phi_c A_c$
A_s	$(1-\phi_c)A_c$
Axial D	D/q, q = tortuosity factor
S	Empirical surface area (m^2/g) multiplied by ρA_c
$8\pi/A_g$ in $\Delta P/P$ formula	Empirical permeability B

The areas in Table 2 do not correspond in an absolute sense, but the substitutions apply to ratios of areas. For uniformly sized spherical particles of diameter d_p, S can be estimated as

$$S = \frac{6A_c}{d_p}(1-\phi_c) \tag{102}$$

This is the sphere surface-to-volume ratio multiplied by the ratio of sphere volume to total volume, and by A_c to obtain surface area per unit length. The tortuosity is a dimensionless number representing the increased path length for diffusion imposed by the irregular flow paths through the column. It is not expected that an open-tube model can predict the results of a packed column experiment, but it may aid understanding of how a packed column experiment might behave if it had a more regular geometry, and lower pressure drop. For example, a comparable tube geometry to the Foltz and Melius experiment[2] would be an array of about 17,000 tubes with 47 μm inside diameter and 76 μm outside diameter, and a gas velocity of about 60 cm/s, requiring about 3x lower pressure drop (130 as opposed to 440 Torr). Modeling of one such tube by the approaches described here could add insight into the interpretation of this experiment.

6.4. Finite pressure drop in a tube

Though a tube is expected to have a lower pressure drop than a similarly performing packed column, and this report has focused on cases of low $\Delta P/P$, it is still useful to consider the consequences of a larger pressure drop, because this can affect choices of tube radius and gas velocity. The key aspects have been pointed out by Golay[1,31] and important concepts are presented in Section 2.4. Because both the diffusion constant and velocity are inversely proportional to pressure, the ratio v_0/D does not change, even if the pressure (or concentration) varies axially. This means that the plate expressions for axial and radial diffusion, which contain this ratio, do not vary axially. Similarly, the ratio v_0/k' does not change, so if $k' >> 1$, the front velocity does not vary axially. However, the kinetic and solid-phase diffusion terms broaden with increasing velocity, and velocity increases along the tube as pressure decreases. If it is desired to maintain the sharpest possible front width for the full duration of an experiment, this could be obtained by keeping the gas velocity in the vicinity of the front near the optimal value. If the pressure drop is significant, this would require slowing the gas velocity (and reducing the

applied pressure) as elution is approached. The case of a finite pressure drop is also compatible with the optimization scenario presented in Section 4.5, where rapid elution of a sharp front is desired, but the shape of the front within the column is unimportant. In this case, a higher-than-optimal gas velocity is applied until shortly before elution. At that point, the exit velocity (as opposed to the axially independent velocity described in 4.5) is reduced to near its optimal value, as estimated from the plate expressions. A finite pressure drop certainly complicates attempts to apply analytical approaches such as the Thomas equation, but this scenario is still conceptually and numerically tractable, and its consideration can lead to column designs with improved performance versus the optimal constant-pressure case.

7. SUMMARY

This report combines the theories of mass transport in open-tube gas chromatography with that of chemical reaction kinetics in ion exchange chromatography. This combination is applicable to hydrogen isotopic displacement chromatography in an open tube. The report describes how a tube is expected to behave under a wide range of operating conditions and geometries, and shows how to obtain performance where the system is either robustly limited by chemical reaction kinetics, or optimized to obtain elution fronts with optimal sharpness, or an optimal amount of sharpness generated per unit time. Computational analysis and design tools could easily be implemented with the information provided here.

The model includes many simplifications, with the goals of making the process easy to understand, and allowing rapid computations that provide good estimates of performance. In a real metal hydride tube, there will be a pressure drop, which could cause a system to be suboptimal over much of its range, and be diffusion-limited at one end and kinetically limited at the other, for example. There is no attempt here to account for isotope-dependent gas transport parameters like diffusion constant and viscosity, parameters that can vary by approximately 50% between isotopes. The solid hydrides can have pressure- and isotope-dependent capacities, so C_s is not necessarily a constant. For some hydrides, especially in the context of preparative-scale chromatography, the isothermal approximation may not be realistic. Despite these limitations, the simple model presented here can still be a useful first pass in a design that can be validated using more sophisticated models.[9,32] The neglect of solid-phase diffusion is shown to be unrealistic for thick tube walls, but porosity in that wall can eliminate this mass transport limitation.

8. REFERENCES AND NOTES

[1] M.J.E. Golay, Theory of Chromatography in Open and Coated Tubular Columns with Round and Rectangular Cross Sections, in Gas Chromatography 1958: Proceedings of the Second Symposium, D.H. Desty, ed., p. 36-55.

[2] G.W. Foltz and C.F. Melius, Studies of Isotopic Exchange Between Gaseous Hydrogen and Palladium Hydride Powder, J. Catalysis 108 409-425 (1987)

[3] M. Li, W.F. Yang, Highly porous palladium bulk: Preparation and properties as active metal material for displacement chromatographic process. Int. J. Hydrogen Energy 34 (2009) 1585-1589.

[4] S. Fukada, K. Fuchinoue, M. Nishikawa, Isotope separation factor and isotopic exchange rate between hydrogen and deuterium of palladium. J. Nuc. Mater. 226 (1995) 311-318.

[5] F. Strzelczyk, D. Leterq, A.M. Wilhelm, A. Steinbrunn. Gas-solid chromatographic separation of hydrogen isotopes: a comparison between two palladium-bearing materials – alumina and kieselguhr. J. Chromatography A 822 (1998) 326-331.

[6] M. Matsuyama, H. Sugiyama, M. Hara, K. Watanabe. Applicability of Pd-Cu alloy to self-developing gas chromatography of hydrogen isotopes. J. Nuc. Mater. 367-370, part B, 1096-1101 (2007).

[7] K. Watanabe, M. Matsuyama, T. Kobayashi, S. Taguchi. Gas chromatographic separation of H2-D2 mixtures by Pd-Pt alloy near room temperature. J. Alloys Compounds 257 (1-2) 278-284 (1997).

[8] S. Fukada, H. Matsuo, T. Okunaga, N. Mitsushi. A study of isotopic exchange of hydrogen and deuterium in a $LaNi_3Al_2$ hydride bed. J. Nuc. Mater. 195 (1-2) 191-197 (1992).

[9] A.D. Shugard, G.M. Buffleben, T.A. Johnson, D.B. Robinson. Isotope Exchange between Gaseous Hydrogen and Uranium Hydride Powder. Journal of Nuclear Matererials 447 (1–3) 2014, 304–313

[10] G. Guiochon, A. Felinger, D.G. Shirazi, A. M. Katti. Fundamentals of Preparative and Nonlinear Chromatography, 2nd ed. Academic Press, 2006.

[11] T. Vermeulen, Separation by adsorption methods, in Advances in Chemical Engineering, T. B. Drew and J.W. Hoopes, Jr., eds., vol. II, 147-208, 1958.

[12] S.C. James, J. Hamilton, W.G. Wolfer. Diffusional exchange of isotopes in a metal hydride sphere. Chem. Eng. Sci. 68 (1) 250-257 (2012).

[13] B.M. Andreev, E.P. Magomedbekov, Separation of Hydrogen Isotopes by Chemical isotope Exchange in Systems Involving Metal and Intermetallic Compound Hydrides. Separation Science and Technology 36 (8-9) 2027-2086 (2001).

[14] W.F. Luo, D.F. Cowgill, T.B. Flanagan, Separation Factors for Hydrogen Isotopes in Palladium Hydride. J. Phys. Chem. C 117 13861-13871, 2013.

[15] http://www.chem.arizona.edu/~salzmanr/480a/480ants/collsurf/collsurf.html

[16] F.M. White, Viscous Fluid Flow. McGraw-Hill, New York, 3rd ed., 2006.

[17] A.F. Mills, Mass Transfer. Prentice-Hall, 2001.

[18] A.A. Clifford, Theory of open-tube chromatography: an exact proof of Golay's equations. J. Chrom. 471 (1989) 61-69.

[19] This requires substitution for Clifford's $k_d = kS/C_s A_s$ where the rate constant on the right-hand side is derived from the linear form of the rate law, and the dimensional terms convert Clifford's surface concentration to the concentration in the solid.

[20] C.A. Cramers, H.-G. Janssen, M.M. van Deursen, P.A. Leclercq, High-speed gas chromatography: an overview of various concepts. J. Chromatography A 856, 315-329, 1999.

[21] In this section, the fraction 11/24 is approximated as 1/2, and $\alpha k'$ is assumed large.

[22] J.E. Walter, Multiple Adsorption from Solutions, J. Chem. Phys. 13 (6) 229-235, 1945.

[23] J.E. Walter, Rate-dependent chromatographic adsorption, J. Chem. Phys. 13 (6) 235-336, 1945.

[24] H.C. Thomas, Heterogeneous Ion Exchange in a Flowing System. J. Am. Chem. Soc. 66 (1944) 1664-1666.

[25] N. K. Hiester and T. Vermeulen, Saturation performance of ion-exchange and adsorption columns. Chem. Eng. Prog. 48 (10) 505-516, 1952.

[26] A. Patton, B. D. Crittenden, S. P. Perera, Use of the Linear Driving Force Approximation to Guide the Design of Monolithic Adsorbents. Chem. Eng. Res. Des. 82 (A8) 999-1009, 2004.

[27] J. Newman, K. E. Thomas-Alyea. Electrochemical Systems. 3rd ed. Wiley, 2004.

[28] The flux discontinuity can be implemented in COMSOL using the internal variable *Hr*, which is the average of $\partial H/\partial r$ in the mobile phase and $\partial(\phi H)/\partial r$ in the stationary phase. Assuming no discontinuity in $\partial H/\partial r$ (which requires assuming rapid equilibration with the solid at the surface) this can be rearranged so the net flux into the mobile phase is specified as $-2[(1-\phi)/(1+\phi)]D\,Hr$.

[29] A. M. Berezhovskii, A. V. Barzykin, V. Yu. Zitserman, "One-dimensional description of diffusion in a tube of abruptly changing diameter: Boundary homogenization based approach", J. Chem. Phys. 131 224110 (2009)

[30] D. K. Schisla, H.B. Ding, P.W. Carr, E.L. Cussler, Polydisperse Tube Diameters Compromise Multiple Open Tubular Chromatography. AIChE J., 39 (6) 946-953, 1993.

[31] M.J.E. Golay, A problem of optimization in capillary gas chromatography. J. Chromatography 348 (1985) 416-420.

[32] R.S. Larson, S.C. James, R.H. Nilson. Isotope Exchange Kinetics in Metal Hydrides I: TPLUG Model. Sandia report 2011-3243, May 2011. DOI: 10.2172/1030413

Distribution

3	MS9291	David B. Robinson	8651
1	MS9158	Maher Salloum	8961
1	MS9035	Steve Rice	8254
1	MS9035	Andrew Shugard	8254
1	MS9161	Weifang Luo	8252
1	MS0899	Technical Library	9536 (electronic copy)


Sandia National Laboratories